



Unraveling the climate control on debris-free glacier evolution in the Everest region (Nepal, central Himalaya) during the Holocene

Vincent Jomelli, Patrick Wagon, Didier Swingedouw, Joanna Charton, Régis Braucher, Adèle Hue, Fanny Brun, Christophe Colin, Stephanie Gairoard, Dibas Shrestha, et al.

► To cite this version:

Vincent Jomelli, Patrick Wagon, Didier Swingedouw, Joanna Charton, Régis Braucher, et al.. Unraveling the climate control on debris-free glacier evolution in the Everest region (Nepal, central Himalaya) during the Holocene. *Quaternary Science Reviews*, 2023, 310, pp.108109. 10.1016/j.quascirev.2023.108109 . hal-04097595

HAL Id: hal-04097595

<https://hal.science/hal-04097595>

Submitted on 15 May 2023

HAL is a multi-disciplinary open access archive for the deposit and dissemination of scientific research documents, whether they are published or not. The documents may come from teaching and research institutions in France or abroad, or from public or private research centers.

L'archive ouverte pluridisciplinaire **HAL**, est destinée au dépôt et à la diffusion de documents scientifiques de niveau recherche, publiés ou non, émanant des établissements d'enseignement et de recherche français ou étrangers, des laboratoires publics ou privés.

- Holocene glacier fluctuations in Himalaya remain puzzling
- We investigate the evolution of two debris-free glaciers in the Everest region
- Glacier chronologies are based on 51 ^{10}Be ages from moraines and roche moutonnees
- The two glaciers show their largest Holocene extent in the Early Holocene.
- We do not observe any moraine from the Mid-Holocene
- Several minor advances are recorded during the Late Holocene
- This pattern does not perfectly conform current knowledge on Asian monsoon changes

Unraveling the climate control on debris-free glacier evolution in the Everest region (Nepal,
Central Himalaya) during the Holocene

Vincent Jomelli¹* Patrick Wagnon², Didier Swingedouw³, Joanna Charton¹, Régis Braucher¹,
Adèle Hue¹, Fanny Brun², Christophe Colin⁴, Stephanie Gairoard¹, Dibas Shrestha⁵, Aster
TEAM*

1. Aix-Marseille University, CNRS, IRD, Coll. France, INRAE, CEREGE, 13545 Aix-en-Provence, France, * corresponding author jomelli@cerege.fr

2. Univ. Grenoble Alpes, CNRS, IRD, INRAE, IGE, F-38000 Grenoble, France

3. Environnements et Paléoenvironnements Océaniques et Continentaux (EPOC),
UMR CNRS 5805, EPOC-OASU Université de Bordeaux, Allée Geoffroy
Saint-Hilaire, 33615 Pessac, France

4. Université Paris-Saclay, CNRS, GEOPS, 91405, Orsay, France

5. Central Department of Hydrology and Meteorology, Tribhuvan University,
Kathmandu, Nepal

*Aster Team members: Georges Aumaître, Karim Keddadouche, Fawzi Zaidi

Keywords: Nepalese glacier, 10Be chronology, Holocene, AMOC, Indian monsoon.

Abstract

Current mass balance and meteorological surveys of Mera glacier located about 30 km south of
Mount Everest in Nepal show the dominant role of Asian monsoon precipitation on interannual
mass balance variability while temperature controls the altitude of snow-rain threshold. As

these observations on mass balance variability only explore the recent decades, studies on paleo glacial extents are useful to investigate the long-term climate forcing on glacier evolution. To do so, we investigated the long-term evolution of the debris-free Mera glacier and a neighbouring small debris-free South Khare glacier. Fifty-one ^{10}Be CRE ages were obtained from samples collected on moraine boulders and roches moutonnées. ^{10}Be CRE ages of the boulders span from the end of the Lateglacial (19.0 – 11.7 ka) to the Little Ice Age (~ 0.6 -0.1 ka). The oldest dated moraine in this study was observed at the base of South Khare glacier with an age of 13.6 ± 0.5 ka. The two glaciers subsequently experienced their largest Holocene extent in the Early Holocene with moraines dated to 11.0 ± 0.3 ka at the base of Mera glacier and 10.8 ± 0.5 ka at the base of South Khare glacier. We did not observe any moraine from the Mid-Holocene. During the Late Holocene several glacier advances were recorded around 2.3 ± 0.2 ka, 1.5 ka and then during the last centuries at Mera glacier and around 2.8 ± 0.6 ka, and during the Little Ice Age at South Khare glacier. To explore the links between long-term Nepalese glacier changes and climate, we used oceanic and terrestrial Indian Summer monsoon reconstructions and temperature and precipitation output from two transient global climate models TraCE and LOVECLIM. These climate data outputs were corrected by a reconstruction of the Atlantic Meridional Overturning Circulation (AMOC) over the Holocene and its associated climatic impacts. We also used sensitivity experiments from the IPSL (Institut Pierre Simon Laplace) model to discuss the possible influence of horizontal resolution, land hydrology, vegetation and runoff on changes in Asian summer monsoon. Importantly, we show this long-term Nepalese glacier pattern does not perfectly conform neither to the Indian monsoon precipitation that is documented from terrestrial and marine records nor to temperature and precipitation changes simulated by the models. While the maximum glacier extent in the Early Holocene corresponds to enhanced precipitation documented by proxies and models, the Late Holocene glacier advance remains puzzling. We claim that new paleo glacier

records and improved climate simulations are necessary to get a better understanding of past glacier changes and the associated climate dynamics, which might be crucial to gain confidence in both glacier and climate future evolutions.

1-Introduction

Over the last decades the recent evolution of the High Mountain Asian (HMA) glaciers mass balance has been widely investigated as they contribute importantly to water resources for approximately 800 million people and are a component of global sea level rise (Brun et al., 2017; Pritchard, 2019; Azam et al., 2021). Recent studies covering most HMA glaciers have revealed an overall mass loss over the last decades with values about -0.18 ± 0.04 m of water equivalent per year (w.e. yr^{-1}) with strong spatial and individual glacier mass balance variability (Brun et al 2017; Hugonnet et al., 2021).

This large spatio-temporal mass balance variability is mainly due to climate and geomorphological causes. Along the HMA temperature and precipitation vary spatially and temporally, leading to heterogeneous climate change and behavior of glaciers (e.g., Sakaï and Fujita 2017; Yan et al., 2018, 2020; Azam et al., 2021). In addition, Sakaï and Fujita (2017) evidenced a spatially variable sensitivity of mass balances of HMA glaciers to temperature while their behavior also depends on precipitation changes.

The other main cause of mass balance variability is related to the geomorphological context of individual glaciers. Brun et al. (2019) have reported that the slope of the glacier tongue, the mean glacier elevation, the percentage of supraglacial debris cover, the avalanche contributing area and the presence of a lake at the base of glaciers all together explain between 11 and 48% of the current mass balance variability.

However, as these contributions only explore the recent decades, studies on paleo glacial extents during the Holocene and older periods are needed to investigate potential influence of

long-term climate forcing on multi-centennial to millennial glacier evolution and thus offer an opportunity to put the recent glacier decline in a longer perspective.

Previous studies that investigated glacier fluctuations during the Lateglacial and the Holocene (11.7 ka - present) using *in situ* produced ^{10}Be cosmic ray exposure (CRE) ages have shown that the multi-centennial glacier evolution differs across the HMA.

This is assumed to reflect the spatial variability of precipitation and temperature as currently observed. This is related to relative influence of the mid-latitude westerlies, the Indian Summer Monsoon (ISM) and the East Asian Summer Monsoon (ESM) (Owen et al., 2008, 2009; Owen, 2009; Owen and Dortch, 2014; Saha et al., 2019). While the mid-latitude westerlies might significantly influence the western end of the range and Tibet (Mölg et al., 2014), the ISM and ESM both combined in the Asian Summer Monsoon are believed to largely dominate the southern and eastern regions, and to a lesser extent the interior (continental) portions of the HMA.

As it is observed that the geomorphological context has influence on mass balance variability over the current period, this geomorphological context should also be considered while investigating long-term glacier change. For instance, in the Khumbu valley, (Everest region, Nepal) previous studies of glacier fluctuations from the Lateglacial were conducted on large debris-covered glaciers (Finkel et al., 2003; Hornsey et al., 2022). However, a detailed understanding of the Lateglacial-Holocene glacier history from debris-free glaciers in the central Himalaya is lacking (Saha et al., 2019). Thus it remains still unclear if the debris cover in the ablation zone may have influenced the long-term glacier response to climate change compared to debris-free glaciers (Owen et al., 2005).

In this context we investigated the fluctuations of two debris-free glaciers in Nepal (Everest region (Fig.1)), based on 51 ^{10}Be CRE ages determined from rock samples of moraine boulders (n=43) and roche moutonnées (n=8) whose ages span the Lateglacial and the Holocene. The

main goals of this study are to document major periods of advances of these two glaciers at a multi-centennial time scale during the Holocene, to compare this signal with other glaciers in Nepal and investigate the potential long-term climate forcings responsible for their evolution. Among the two investigated glaciers, the Mera glacier is an ideal target to explore long-term glacier-climate relationship and compare long-term vs. short-term glacier response to climate change. Indeed, on this glacier an understanding of physical processes driving current mass balance has been led through mass and energy balances surveys since 2007 (Wagon et al., 2013; 2021; Sherpa et al., 2017; Litt et al., 2019). The originality of this study is thus to combine different approaches i.e., surface process understanding at present, as well as moraine dating, climate reconstructions and climate model outputs over the Lateglacial-Holocene period, to unravel the climate control on debris-free glacier evolution in the Everest region. The study area, moraine stratigraphy and the climate setting are presented in section 2. Based on the methodology described in section 3, CRE moraine ages are presented in section 4. In section 5-1, 5-2 and 5-3 we discuss our moraine records and compare the two chronologies with other studies conducted in Nepal and in other regions of HMA respectively. In section 5-4 we discuss potential forcings driving the evolution of the two investigated glaciers.

2- Study Area and climate setting

2-1 Physical setting

The two investigated Mera (ME) and South Khare (SK) glaciers are located in the upper Dudh Koshi basin, at about 30 km south of Everest summit (central Himalaya, 27°.74 Lat; 86°.86 Long) (Fig. 1). In this area the bedrock is dominated by quartz-rich granite and gneiss. Mera glacier is a debris-free summer-accumulation glacier type with an area of 4.84 ± 0.34 km² in 2018 and a maximum altitude of 6420 m a.s.l. (Wagon et al., 2021). The glacier extends northwards and divides into two branches at 5800 m a.s.l.. The main branch, oriented north-

west, with a mean slope of $\sim 16^\circ$, goes down to 4910 m a.s.l. at snout. Here, samples from several moraines were collected. The minor Naulek branch, oriented north-east was not investigated in this study. Mera glacier mass balance has been investigated both using the classical glaciological (stakes) method since 2007 and more recently the geodetic method (Wagnon et al., 2013; 2021). Annual and seasonal measurements of the glacier mass balance showed that the accumulation and ablation processes happen during the same monsoon period. There is limited mass change during the dry, cold and windy winter, apart from wind ablation and sublimation (Sherpa et al., 2017; Litt et al., 2019; Wagnon et al., 2021). The glacier-wide mass balance calibrated over geodetic mass balance was slightly negative for the period 2007-2013 (MB -0.23 ± 0.23 m w.e./yr) with more negative values for the period 2013-2020 (-0.57 ± 0.19 m w.e./yr) (Wagnon et al., 2021). In addition the mass balance variations of this glacier are in agreement with observations conducted at a regional scale (Hugonnet et al 2021). Thus, it can be seen as representative of the regional trend. Mera glacier is bounded by six distinct lateral moraines, which were named, from the right to the left side of the glacier looking downhill, M1 for the youngest to M₆ for the oldest i.e. Mera ME-M1 to M6 (Figs. 2, 3). A large terminal moraine over 200 m wide formed by the nested crests (ME-M1, -M2, -M3), is cut by a small river from the glacier with a frontal ramp 50 m in relief (Figs 2, 3). On the right side of the Mera glacier about 400 m downstream from the front and about 200 m below in altitude, two large lateral moraines are visible. The inner one is composed of the three nested ridges (ME-M1, -M2, -M3). The ME-M1 lateral moraine is continuous over about 1.5 km from the terminus and is actually superimposed on two other lateral moraines ME-M2 and ME-M3 and certainly explains its large relief. The ME-M1 moraine has unvegetated or poorly vegetated surfaces and unstable proximal slopes with crest heights up to 80 m above the proglacial sandur formed by the river flowing from the front of the glacier. The Mera ME-M2 and ME-M3 right lateral moraines are fragmented and only identifiable from 200 m and 500 m respectively up-

glacier from the terminus. Both crests are separated by 10–50 m horizontally from the Mera moraine ME-M1 and at a lower altitude (30 and 50 m respectively). The distal slope of these two moraines is steep but stable and vegetated. The relief of these two ridges is not well developed and generally does not exceed 3 m in height.

Distant to about 200 m from the rampart towards the north, separated by approximately 50 m horizontally from ME-M3, an older lateral moraine (ME-M4) is totally covered by vegetation. This lateral moraine shows two distinct crests and only the distal one has been investigated. This right lateral ME-M4 moraine has an asymmetrical cross-profile with a rather flat surface and a steep but stable, vegetated distal slope (Figs 2, 3).

Downslope the moraine ME-M4 was probably connected to the lateral moraine of South Khare glacier. The crest is rounded and has a relief of about 20 m above the valley floor. Moraines on the left side of the glacier are less well preserved. Only two ridges were investigated. One is relatively fresh in shape (ME-M5) while the other (ME-M6) is also covered by vegetation. From the terminus of the frontal moraine a fragmented ridge is only identifiable over about 100 m toward the glacier. At an altitude of about 4750 m a.s.l. the ridge of ME-M5 is buried by another moraine which was not studied. This part of the left side of the glacier was also impacted by dirty snow avalanches and was not deeper investigated. The relief of this left lateral moraine ME-M5 is about 50 m above the valley. ME-M6 moraine is only preserved from periglacial processes over a distance of approximately 100 m. This vegetated moraine constitutes the most external ridge of the rampart on the left side of the glacier. On the inner side of these two moraines, several ridges are visible but are too steep to be sampled.

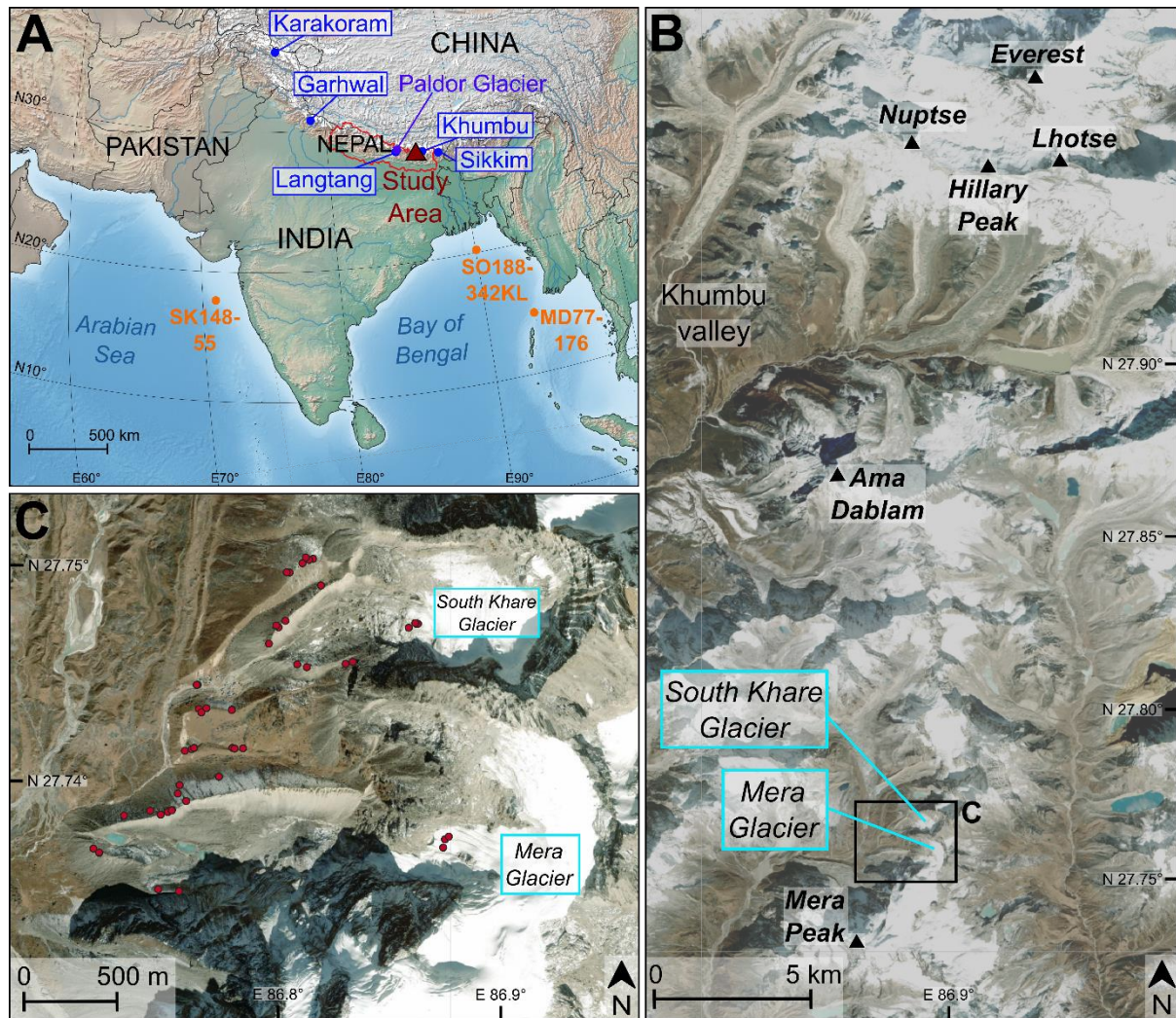


Figure 1. Location map of Mera and South Khare glaciers (blue frames) and other relevant locations presented throughout the study (black triangles correspond to the summits) in the upper Dudh Koshi basin, Everest region (central Himalaya). a). The inset shows the study area (red triangle) in the High Mountain Asia. Blue dots correspond to the different regions of the HMA, the purple dot shows another glacier cited in this study and orange dots show the location of marine cores discussed in the text. b). Debris free and debris-covered discussed in this study. c). Mera and Shouth Kare moraine records with sample locations (red dots).

South Khare glacier (0.47 km^2) is located 1 km north of Mera glacier and has a catchment area of $\sim 2.7 \text{ km}^2$ with an elevation ranging from $\sim 5200 \text{ m a.s.l}$ at the front to $\sim 5890 \text{ m a.s.l}$ at the

top (Fig. 1). It is also a debris-free glacier facing west with a mean slope of $\sim 17^\circ$. At the base of South Khare glacier, the configuration of the moraines is rather similar to that of Mera glacier with eight identified moraines the SK M1–8 moraines, with each crest separated by 2–70 m horizontally (Figs. 4, 5). At a distance of ~ 700 m down-valley from the current front position, a large rampart of about 60 m high is composed of at least two young nested lateral moraines with individual crests (SK-M1, -M2 on the right side, -M6, -M7 on the left side) that were sampled at both sides of the valley. The South Khare right lateral moraine SK-M1 is continuous along the right of the glacier with an elevation ranging from 5010 to 5200 m a.s.l. Down-valley of the right side of the glacier, two distinct crests (SK-M3, -M5) were investigated. The youngest crest forms a continuous right lateral moraine SK-M3 of about 300 m in length. The relief of this lateral moraine exceeds 50 m. The steep proximal slope is dissected by relict and active gullies while the distal slope shows only very few boulders with a sub horizontal surface. A remnant ridge SK-M5 of 2 m in relief on the right side of the glacier is distant to about 10 m from SK-M3 horizontally. This discontinuous ridge is only visible near the ablation zone while downslope the crest connected to the lateral moraine SK-M4 disappears. On the left side of the glacier two crests are also visible on the upper part of the ablation area close to each other horizontally. The uppermost ridge SK-M6 forms a continuous crest of about 50 m in relief with a symmetric cross profile. The altitude of this ridge between 5000 and 5150 is the same as SK-M1 on the right side of the glacier. This moraine is up to 80 m in relief dominating the village of Khare. On the distal slope of the ridge another discontinuous crest SK-M7 is visible at about 5040 m a.s.l. over a distance of 50 m. Approximately 150 m horizontally towards the south from SK-M7 an old vegetated and rounded moraine SK-M8 of about 30–50 m in relief is visible.

209

210 2-2 Climate Setting

211 The Everest region is under the influence of the ISM, when approximately three quarters of the
212 annual precipitation fall during the summer months from June to September (Litt et al., 2019;
213 Perry et al., 2020). For the year 2019-2020, the Northern Bay of Bengal is the most important
214 source of moisture during the monsoon (62 %), more than from the Indus River Delta and
215 Arabian Sea (21 %) and Indo-Gangetic Plain (17%) (Perry et al., 2020). From October to May,
216 the westerlies on the continent are predominant for precipitation (Perry et al., 2020). The
217 monsoon usually stops suddenly at the end of September/beginning of October when the
218 weather, mostly cloudy, calm and warm with frequent precipitation switches within a few days
219 to constantly sunny and dry conditions, progressively colder and windier, during the post
220 monsoon (October-November). Very dry, sunny and windy conditions prevail during the winter
221 (December - February) where there is almost neither any clouds nor precipitation. From March
222 to May, the pre-monsoon is characterized by a progressive increase in convective clouds
223 bringing warm and humid air, with progressively more and more precipitation and a decrease
224 in strong winds (Bookhagen and Burbank, 2006; Sherpa et al., 2017; Khadka et al., 2021).

225

226 2-3 Processes controlling the glacier mass balance

227 In this Indian monsoon-dominated region, over **debris-free** glaciers, ablation is dominated by
228 melt in the lower part of the glacier **below** the equilibrium line altitude (ELA) above which
229 sublimation plays a substantial role during all seasons, except the monsoon (e.g. Wagnon et al,
230 2013; Stigter et al., 2018; Litt et al., 2019; Fugger et al., 2022). The radiation budget mostly
231 controls the melt (Stigter et al., 2021). The incoming shortwave radiation is maximal during the
232 pre-monsoon, before the installation of permanently overcast conditions during the monsoon,
233 responsible for maximal incoming longwave radiation compensating the heat loss *via* outgoing

longwave radiation (Bonekamp et al, 2019; Matthews et al, 2020). Overall, the net all-wave radiation is high during the pre-monsoon and monsoon and is controlled by the albedo and by the seasonality of cloudiness (the percentage of cloud in a given atmospheric layer) (Bonekamp et al., 2019; Stigter et al., 2021). Snow with its impact on albedo and air temperature and its control on the rain-snow limit, are therefore very important meteorological variables influencing the glacier mass balance in the ablation area. Wind speed, which governs sublimation, is more important in the accumulation area. Most of the ablation still happens during the monsoon due to stronger melt than during the pre-monsoon season, when refreezing compensates the melt until the cold content of the glacier surface layers originating from the winter has been evacuated (e.g., Fugger et al., 2022).

3- Methods

3-1 Field sampling

The field campaigns took place in 2014, 2016 and 2018. Moraines were sampled and mapped in the field using a Garmin GPS survey instrument (precision 10 m) (Table 1). Using a hammer and a chisel, 51 granitic boulders (> 60 cm in height) were sampled from the crest of the 14 selected moraines and on roches moutonnées (bedrock) close to the front of the glaciers. A Suunto Compass Clinometer PM-5 was used to measure topographic shielding for each sample in the field. Sample elevation was extracted from the handheld Garmin GPS instrument. All the boulders were photographed and their ground-to-sample height was measured. We have considered well-preserved moraines (> 1 m high and > 20 m long), and selected boulders and locations on the moraine with no evidence of disturbance caused by the action of other processes (river, rock fall or debris flow; Jomelli and Francou 2000). In order to document the deglaciation chronology of Mera (ME) and South Khare (SK) glaciers, we first collected samples on roches moutonnées close to their current front position (Figs 2-

5). Other samples were collected downslope on lateral moraines at approximately 1-2 km from the current front.

3-2 Sample preparation and AMS measurement

All samples were processed at CEREGE (Aix-en-Provence, France). Samples were crushed and sieved to collect the 250-1000 μm fraction. Quartz was first concentrated by magnetic separation and then isolated by successive leaching in a $\frac{2}{3}$ H_2SiF_6 / $\frac{1}{3}$ HCl mixture. The obtained quartz fraction was leached at least 3 times in a 10% HF - 10% HNO_3 solution, in order to remove any remaining feldspars and to clean the grains from atmospheric ^{10}Be . Purified quartz was completely dissolved in concentrated HF (48%) after addition of an in-house ^9Be carrier solution (3025 ± 9 ppm; Merchel et al., 2008). Beryllium was extracted by successive alkaline precipitations of $\text{Be}(\text{OH})_2$ alternated with separation on anion and cation columns. Samples were then oxidized at 700°C for 1 hour and the final BeO mixed with Nb powder and loaded into copper cathodes. AMS measurements of the $^{10}\text{Be}/^9\text{Be}$ ratios were conducted at the French national AMS facility ASTER (Arnold et al., 2010). Samples were calibrated against the in-house standard STD-11 ($^{10}\text{Be}/^9\text{Be} = 1.191 \pm 0.013 \cdot 10^{-11}$; Braucher et al., 2015) and a ^{10}Be half-life of $1.387 \pm 0.0012 \cdot 10^6$ years (Chmeleff et al., 2010; Korschinek et al., 2010). Analytical uncertainties combine ASTER counting statistics, standard uncertainty, external uncertainty (0.5%; Arnold et al., 2010) and machine blank correction. ^{10}Be concentration in the sample was calculated from the corresponding $^{10}\text{Be}/^9\text{Be}$ ratio and was corrected from associated chemical blanks (Table 1). Scaling to the sample locations was made according to the recent, physically-based, LSD model (Lifton et al., 2014) which performs similarly to older empirical models presented in Borchers et al., (2016). Chosen parameters include the ERA 40 atmospheric reanalysis (Uppala et al., 2005) and the VDM 2016 geomagnetic database. We used the SLHL

global production rate of 4.08 ± 0.23 atoms $\text{g}^{-1} \text{yr}^{-1}$ as no regional production rate is available so far.

Exposure ages were computed with the online CREp program (Martin et al., 2017; <http://crep.cirp.cnr-nancy.fr>) and are presented in Table 1. In order to make our results easily comparable to previous studies carried out in other regions of the HMA, we present in Table 2 the exposure ages computed using the time-dependent “Lm” scaling model (Lal, 1991; Stone, 2000) and recalibrated previous data when comparisons were made with previous studies.

^{10}Be CRE ages are reported with 1σ “external” uncertainties, which include measurement, production rate and scaling uncertainties (e.g., Balco et al., 2008), in the main text and on the maps (Figs. 2, 4) for better comparison with other proxies. Both internal and external uncertainties are reported in Table 1. For comparison we have recalculated all moraine ages using the different tests such as Chevenet’s and Peirce’s referenced in Batbaatar et al. (2018) that are summarized in the table S1. However, for a given moraine, its assigned age corresponds to the weighted mean of the sample ages that successfully passed a Chi^2 test (calculated with the internal uncertainties) used to identify outliers (Ward and Wilson, 1978). Chi^2 test was preferred because it is the most conservative test compared to the others (see Table 1). Based on field observations, we also considered the stratigraphic relationships to identify outliers.

3-3 Paleoclimate data from the two transient model simulations

To explore links between glacier behavior and climate forcings we have used output from two available transient global climate model (GCM) simulations from LOVECLIM (Kobashi et al., 2016) and CCSM4 (Liu et al., 2009). The so-called TraCE simulation from CCSM4 includes variations in insolation, greenhouse gas concentrations, ice sheet extension and altitude from the ICE5-G reconstruction and also a crude estimate of associated freshwater release in the North Atlantic. LOVECLIM uses similar forcings, but ICE-6G for the ice sheet, and does not

account for freshwater release in the North Atlantic. This second transient simulation also includes an estimate of volcanic forcing, which is not included in the TraCE simulation.

As the Atlantic Meridional Overturning Circulation (AMOC) evolution is poorly represented in the two models, we corrected the transient simulations using the Ayache et al. (2018) reconstruction of the AMOC.

The AMOC reconstruction for Ayache et al. (2018) was then calibrated using Northern Hemisphere reconstruction of Kaufman et al. (2020) and transient model simulations as well as hosing simulations from Swingedouw et al. (2013), in order to quantify the climatic impacts of AMOC variations. From there, the variables simulated in the transient run have been corrected using a semi-empirical model described in detail in Jomelli et al. (2022).

For comparative purposes we also included in our analysis Mid-Holocene to present-day evolution of the ISM from other transient global simulations described in detail in Cretat et al., (2020). Here we benefited from sensitivity analyses conducted by the authors who investigated the effects of horizontal resolution, land hydrology, vegetation and runoff on changes in the ISM, with a focus on its seasonality at the monthly time scale and on extremes at the seasonal time scale. They also analyzed changes in the interannual-to-decadal variability of the ISM from two model versions of the IPSL Earth System model.

3-4 Comparison with other moraine chronologies from the HMA

To get a better understanding of glacier fluctuations in the HMA we explored other CRE moraine records from the worldwide Ice-D database (<http://alpine.ice-d.org/>). Here we have applied four criteria to be consistent with the analysis. We did not consider moraines dated with only one CRE age or unpublished data. We focused on glacial valleys without undated moraine that may have been formed during the timeframe investigated in this study. As an example, a

study that would provide an age for a Lateglacial moraine without dating other moraines located upstream would not be conclusive for our purpose and thus would not be considered in the regional comparison. In addition, a moraine dated with ages that show a large dispersion is rejected for the same reason as possibly reflecting inheritance or post depositional changes. Following the same strategy, we did not consider glacial valleys with moraines dated with uncertainties that do not make possible to attribute the moraine formation to a specific period (Lateglacial or Early, Mid or Late Holocene).

4- Results

We present 51 ^{10}Be CRE ages in this contribution, 25 ^{10}Be CRE ages from Mera glacier and 26 ^{10}Be CRE ages from South Khare glacier.

4-1 Mera glacier chronology

The chronology of the Mera glacier is based on samples from roche moutonnées located just a few meters below the current front position of the glacier and from six moraines (Figs. 2, 3). Four samples (D1, D2, D3, D4) were collected on roche moutonnées that were covered by ice until recent years. Apparent CRE ages of these samples range between 0.05 ± 0.03 ka to 0.25 ± 0.09 ka. As these surfaces were covered by ice and therefore protected from cosmic rays, until recent years (this is evidenced in recent aerial photos and successive field trips during which we witnessed the frontal retreat of the glacier) their apparent ages should be null. The apparent young ages for D1 and D4 are probably due to inheritance due to insufficient resetting by ice abrasion since a potential previous exposure or pre-exposure under reduced ice thickness during the last centuries. Five samples (B1, B5, B7, 17nep11 and 17nep12) were taken on this youngest and highest ridge ME-M1. ^{10}Be CRE ages are between 0.06 ± 0.02 ka (B7) and 0.43 ± 0.08 ka (B1). Among these samples, B7 was considered as an outlier based on Chi^2 test and was

excluded from the mean age calculation of the moraine that yields a ^{10}Be CRE age of 0.30 ± 0.03 ka (n=4). Three samples were collected on the Mera right lateral moraine ME-M2. Here we selected the largest boulders and tried to avoid boulders that could have fallen from the moraine ME-M1. These samples B2 (0.75 ± 0.13 ka), B3 (0.90 ± 0.25 ka), and B4 (0.72 ± 0.13 ka) yield a weighted mean ^{10}Be CRE age of 0.8 ± 0.1 ka (n=3). On the third nested right lateral moraine ME-M3, the two samples 17nep10 (1.31 ± 0.25 ka) and 17nep13 (1.71 ± 0.3 ka) yield a mean ^{10}Be CRE age of 1.5 ± 0.2 ka. The right lateral moraine ME-M4 was dated at 11.0 ± 0.3 ka from the weighted mean of six samples (I1, I2, I3, J1, J2, J3) that showed rather consistent ^{10}Be CRE ages ranging between 10.7 ± 0.6 ka and 11.6 ± 1 ka. ME-M5 was dated to 2.3 ± 0.2 ka based on three samples (17nep15, 17nep16 and 17nep17). Finally, the older short ridge left lateral moraine ME-M6 was tentatively dated to 11.3 ± 0.6 ka based on the only sample 17nep20, because 17nep19 age (0.30 ± 0.05 ka) is considered as an outlier based on stratigraphy.

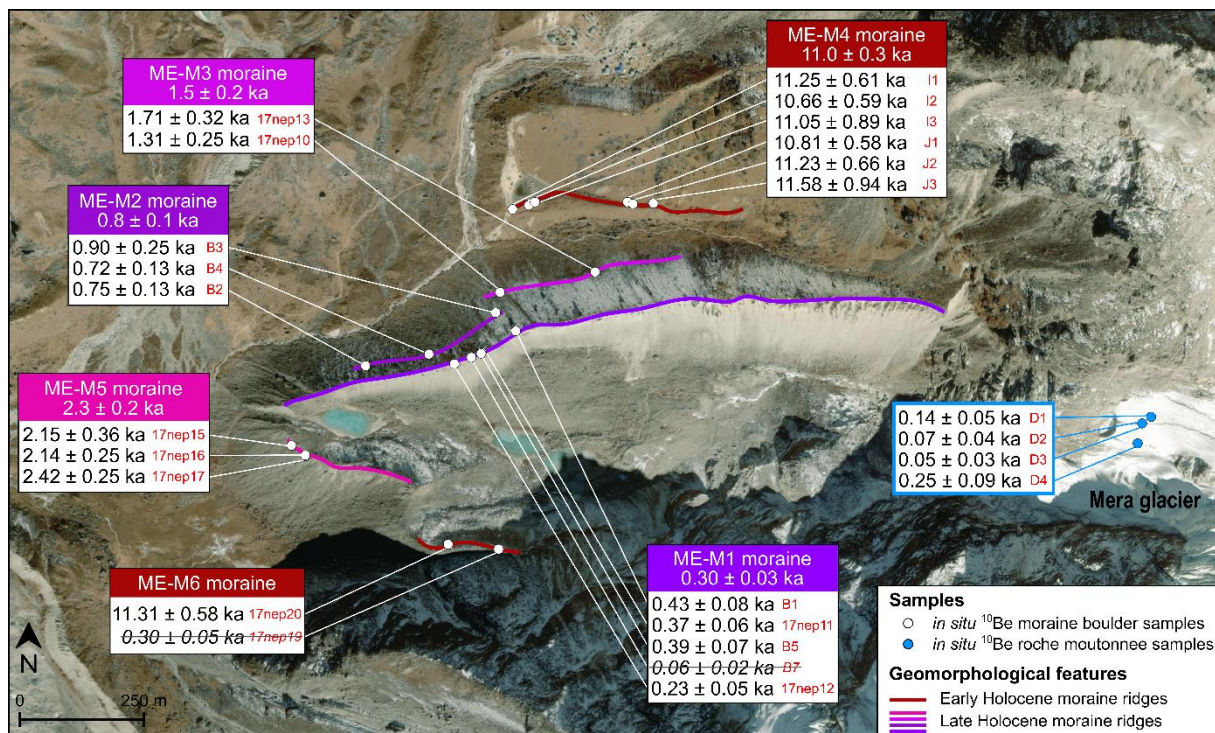


Figure 2. Chronology of the Mera glacier's evolution. Geomorphological features are mapped on aerial imagery of the investigated glacier. White boxes show the ^{10}Be sample ages of moraine boulders and roches moutonnées with their external uncertainties. Samples written in struck-through italic text are rejected as outliers and therefore excluded from the discussion. The weighted mean ages for moraine groups are shown in coloured boxes. **Note that the aerial image used here was taken in the 1990s. ^{10}Be samples from roche moutonnées were collected in 2020 at a location which was covered by ice in the 1990s.**

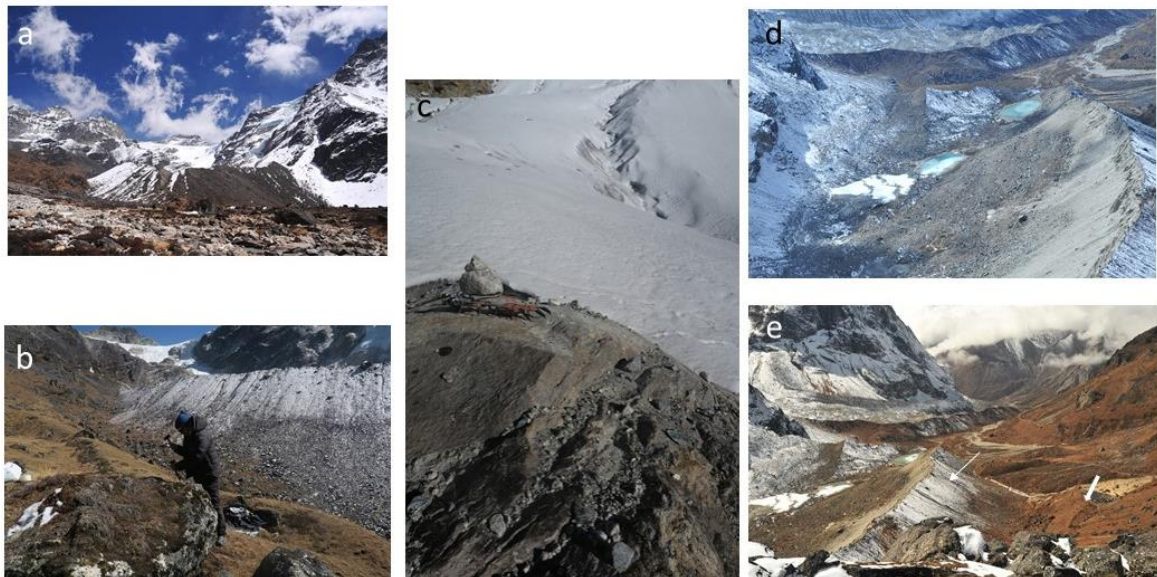


Figure 3. Pictures from Mera catchment and moraines. a). Terminal Late Holocene moraine; b). Sampling on ME-M4 lateral moraine; c). roche moutonnée at the front of the glacier; d). View from the front of the glacier towards the terminal moraine, note the unstable proximal slope of the right lateral moraine M1; e). view from the front of the glacier towards the terminal moraine, note the vegetated lateral right moraine ME-M4 (thick arrow) and the large rampart composed of ME-M1-3 moraines (fine arrow).

4-2 South Khare glacier chronology

Samples were collected on eight moraine ridges and recently ice-free roches moutonnées close to the front of the glacier (Figs. 4, 5). The four samples (C1, C2, C3 and C4) on these roches moutonnées show apparent ages from 0.12 ± 0.04 ka (C3) to 0.4 ± 0.07 ka (C1). Here again these roches moutonnées were covered by ice until recently suggesting some inheritance related to a complex history of the glacier over at least the Holocene or a reduced thickness of ice over the last centuries.

On the crest of moraine SK-M1 of South Khare glacier, 3 samples 17nep5, 17nep7, and 17nep8 were collected on the uppermost part of the ridge. 17nep7 dated to 0.87 ± 0.08 ka is considered as an outlier based on the χ^2 test and therefore rejected from the mean age calculation of SK-M1, that gives a weighted mean ^{10}Be CRE age of 0.36 ± 0.03 ka. At a distance of about 15 m horizontally from the right lateral moraine on the upper ablation area, another lateral ridge is visible towards the north west of the main valley. This right lateral moraine SK-M2 was dated to 2.9 ± 0.3 ka based on two samples (17nep6 and 17nep9). North of this landform, two nested crests forming the large vegetated moraine located on the right side of the glacier were investigated. On the youngest one three large blocks (1-2 m in length) (17nep2, 17nep4 and Mera15) were selected near the upper ablation zone, where the slope of the longitudinal profile of the moraine is gentle. These samples yield a mean weighted ^{10}Be CRE age of 9.7 ± 0.4 ka. At the base and on the proximal slope of SK-M3 two samples H1 (10.49 ± 0.58 ka) and H2 (11.25 ± 0.75 ka) were collected on a remnant ridge of about 100 m long and about 3m in relief. These small blocks (70 -90 cm long) yield a mean ^{10}Be CRE age of 10.8 ± 0.5 ka (SK-M4; $n=2$). Assuming this ridge to be connected to the SK-M3 and considering H2 as an outlier (based on the χ^2 test), the moraine ensemble SK-M3 and SK-M4 would give a mean ^{10}Be CRE age of 9.9 ± 0.2 ka ($n=4$). Finally, three samples were collected on large boulders ($> 1\text{m}$) on the remnant ridge SK-M5 (14nep1, 17nep1 and 17nep3) which show a weighted mean ^{10}Be CRE age of 13.6 ± 0.5 ka ($n=3$).

On the left side of the glacier two samples were collected on the uppermost ridge SK-M6 (Mera7 and Mera9) that yield a mean ^{10}Be CRE age of 0.24 ± 0.04 ka ($n=2$), which is a bit younger than the youngest crest SK-M1 on the right size of the glacier. On the distal slope of the other lateral and discontinuous lateral crest SK-M7 dated to 2.8 ± 0.6 ka ($n=2$) may be synchronous with SK-M2 on the right side of the glacier (dated to 2.9 ± 0.3 ka). This oldest lateral SK-M8 moraine on the left side of the glacier was dated to 12.8 ± 0.5 ka based on the mean of 3 samples (17nep22, G1 and G2).

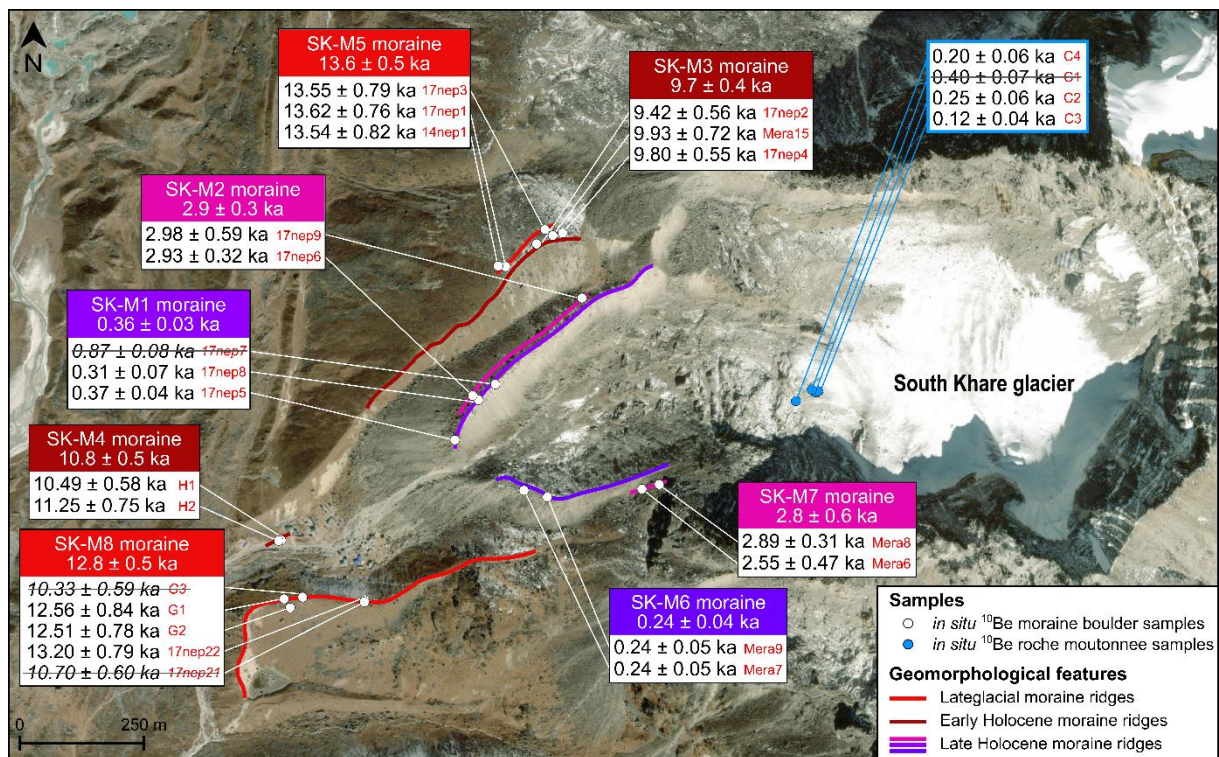


Figure 4. Chronology of the South Khare glacier's evolution. Geomorphological features are mapped on aerial imagery of the investigated glacier. White boxes show the ^{10}Be sample ages of moraine boulders and roches moutonnées with their external uncertainties. Samples written in striked-through italic text are rejected as outliers and therefore excluded from the discussion. The weighted mean ages for moraine groups are shown in coloured boxes.

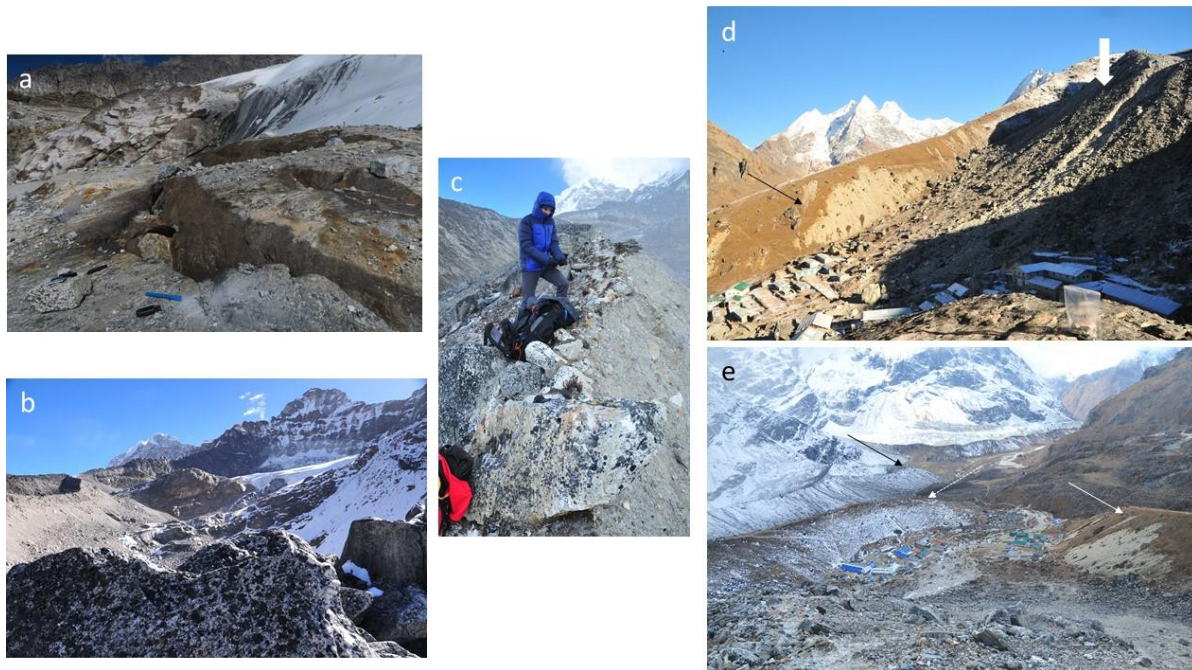


Figure 5. Pictures from South Khare catchment and moraines. a). Roche moutonnée at the base of the glacier. b). Boulder on the lateral left moraine SK-M6; c). Sampling on SK-M1; d). lateral view taken from SK-M8, note at the back the vegetated lateral right moraine SK-M3 (black arrow) and the terminal Late Holocene moraine at the right of the picture (white arrow); e). picture from the front of the glacier towards the village. Showing the right lateral moraine SK-M3 (fine white arrow) and SK-M8 (fine dotted white arrow) and a lateral moraine of Mera glacier black arrow.

5- Discussion

5-1 Evolution of Mera and South Khare glaciers since the Lateglacial

The 51 ^{10}Be CRE ages from samples collected on moraines and roches moutonnées from Mera and South Khare glaciers in the upper Dudh Koshi basin help addressing questions about the Lateglacial and Holocene glacier fluctuations and their related climate conditions in the central Himalaya. The oldest documented moraines are dated to ~ 13 ka (the two oldest moraines at the base of South Khare glacier SK-M5 13.6 ± 0.5 ka; SK-M8 12.8 ± 0.5 ka). SK-M5 may have been formed during the Bølling/Allerød (B/A) (between about 14.7 and 12.9 ka) while SK-M8

may have been formed earlier or during the Younger Dryas (YD) (defined between 12.87 ± 0.3 and 11.61 ± 0.4 ka; Cheng et al., 2020) on South Khare glacier. Field observations suggest that the glacier experienced an almost comparable extent in the Early Holocene ($11.6 - 8$ ka) as revealed by the existence of the nested moraine SK-M3 (9.7 ± 0.4 ka) on the right side of the glacier against SK-M5 and thus was deposited by a glacier of comparable extent. Since no moraine was dated from the end of the Lateglacial so far on Mera glacier, we speculate that the Early Holocene glacier advance experienced by the glacier is also its oldest moraine record over the investigated period. Thus, the behavior of the two glaciers at the end of the Lateglacial remains elusive and more data are needed to better constrain their evolution during the transition between the warm B/A and the YD.

During the Holocene we evidenced that the largest glacial extent occurred in the Early Holocene at $\sim 9-11$ ka on the two glaciers (ME-M4 dated to 11.0 ± 0.3 ka and SK-M3 dated to 9.7 ± 0.4 ka). In addition, we did not find any other moraine formed during the Mid-Holocene ($\sim 8-4$ ka) suggesting the extent of the two glaciers was smaller during this period than during the Late Holocene ($\sim 3-0$ ka). Moreover, apparent ages of roche moutonnées recently uncovered by ice showed some inheritance or potential accumulation through the ice that may corroborate this hypothesis. During the Mid-Holocene the front of the glacier would have been located at a higher altitude than the current altitude favouring ^{10}Be accumulation. During the Late Holocene larger glacier advances than during the Mid-Holocene would have eroded earlier pre-exposed bedrock surfaces but not totally removed ^{10}Be accumulated during these previous Mid-Holocene periods free of ice. One may also hypothesize that ^{10}Be might have accumulated when ice thickness was reduced to a few meters due to energetic muon particles (Dunai, 2010). In such a hypothesis the retreat of the glacier during the Mid-Holocene or periods during the Late Holocene could have just been slightly smaller than the latest Late Holocene glacier advances which caused larger extents evidenced by the dated moraines reported in this study. From about

3 ka, several advances were recorded with at least two advances larger than those occurring during the Little Ice Age on both glacier's margin (Rowan et al., 2016; Solomina et al., 2016). The oldest one may have occurred at about 2.5 ka as suggested by ME-M5 dated to 2.3 ± 0.2 ka on Mera glacier's site, SK-M2 dated to 2.9 ± 0.3 ka and SK-M7 dated to 2.8 ± 0.6 ka on South Khare glacier's site. Another glacier advance period may have occurred at the base of Mera glacier at about 1.5 ka as reported by ME-M3 dated to 1.5 ± 0.2 ka. Finally several advances occurred during the last millennium with ME-M2 dated to 0.8 ± 0.1 ka, and others occurring during the Little Ice Age with SK-M1 dated to 0.36 ± 0.03 ka, ME-M1 dated to 0.3 ± 0.03 ka, and SK-M6 Dated to 0.24 ± 0.04 ka.

Interestingly, the moraines of the investigated glaciers did not vary synchronously at a centennial time scale but revealed a common pattern of change at a millennium time scale. We suspect that these differences in the chronology at a multidecadal time scale may be due to the morphology and topography of the glacier, moraine preservation and uncertainties associated with the CRE ages (Gibbons et al., 1984; Brun et al., 2019). In addition, on the two glaciers, the different extents recorded during the Holocene, in particular during the Late Holocene, have a rather similar amplitude.

5-2 Comparison with other glacier chronologies in Nepal

To make easier comparisons, previous chronologies mentioned below were recalculated following the same cosmogenic approach as the one presented in the method section of this paper (production rate, scaling scheme, atmospheric pressure etc). The two small debris-free glaciers investigated in this study revealed intriguing evolution compared with the evolution of another debris-free Paldor glacier located in Ganesh region, central Nepal (Gayer et al., 2006). We notice that the most significant phase of retreat of the debris-free Paldor glacier in Ganesh

region (central Nepal), occurred before the Early Holocene (Gayer et al., 2006) (Figs.1, n°5 on fig. 6). This rapid reduction in ice volume was followed by a relative stability of Paldor glacier extent around 11 ka. A second phase of retreat starting soon after 8.5 ka, with a minor readvance during the recent centuries, is suggesting comparable glacier behavior in Ganesh and Everest regions.

On the other hand, in the Khumbu valley, two moraines formed by the debris-covered glacier flowing from Hillary peak in between the Nuptse and Lhotse summits are dated to the Last Glacial Maximum (Finkel et al., 2003) defined between 26.5 ka and 19 ka (Clark et al., 2009) and the Late Holocene respectively. These results show that the maximum Holocene ice extent of this debris-covered glacier occurred during the Late Holocene. This suggests that this glacier would have another pattern of change compared to the debris-covered Khumbu glacier (with a maximum extent dated to ~7 ka) and the two debris-free glaciers investigated in this study.

However, more data are needed before being conclusive as undated moraines located in between the Last Glacial Maximum and the Late Holocene exist (this is the reason why we excluded such a case with undated moraines for our comparison). In addition, the age of two moraines downslope from the debris tongue at the base of the northern face of Ama Dablam (Fig. 1; n°7 on Fig.6) investigated by Finkel et al. (2003) reveals that the glacier formed a massive moraine during the YD-Early Holocene transition (~12-11 ka) and another one during the Late Holocene respectively (n°7 on Fig. 6). Thus, the debris-covered tongue of Ama Dablam glacier would show a potentially similar evolution at a millennial time scale with the two debris-free glaciers investigated in this study if one assumes the massive moraine to be formed during the Early Holocene. Finally, the Chhukung stage moraine (defining Early Holocene advance) at the base of the debris-covered Khumbu glacier (n°9 on Fig. 6; Finkel et al., 2003) shows ages from the YD using the same calculation criteria (LSD, VDM, ERA 40 and the same production rate). However, recent investigations on the lateral moraines of Khumbu (n°9 on

Fig. 6) suggest a maximum Holocene extent during the Mid-Holocene which is asynchronous with that of the adjacent Lobuche glacier (n°8 on Fig. 6) occurring during the Late Holocene (Hornsey et al., 2022). Thus, despite this remarkable pioneer work conducted about 20 years ago in the Everest region (Finkel et al., 2003) and more recent investigations, it remains difficult to compare the evolution of debris-free and debris-covered glaciers as more data are needed to be conclusive. Nevertheless, some moraines of the Late Holocene observed on Mera and South Khare glaciers were also documented on the two Khumbu and Lobuche glaciers (Hornsey et al., 2022

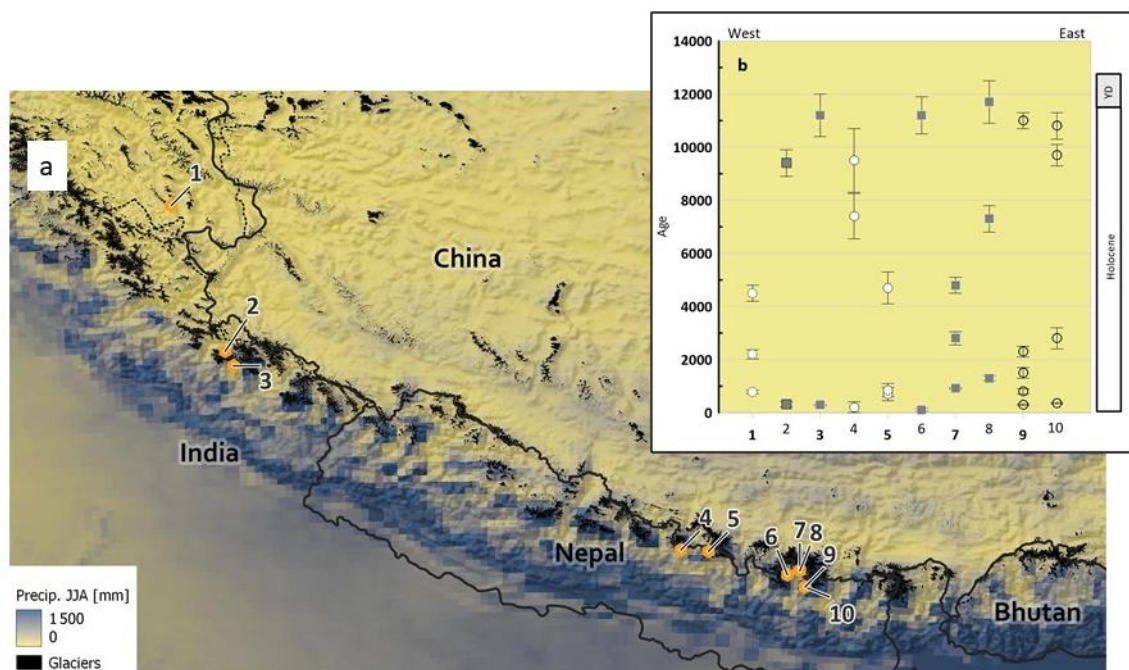
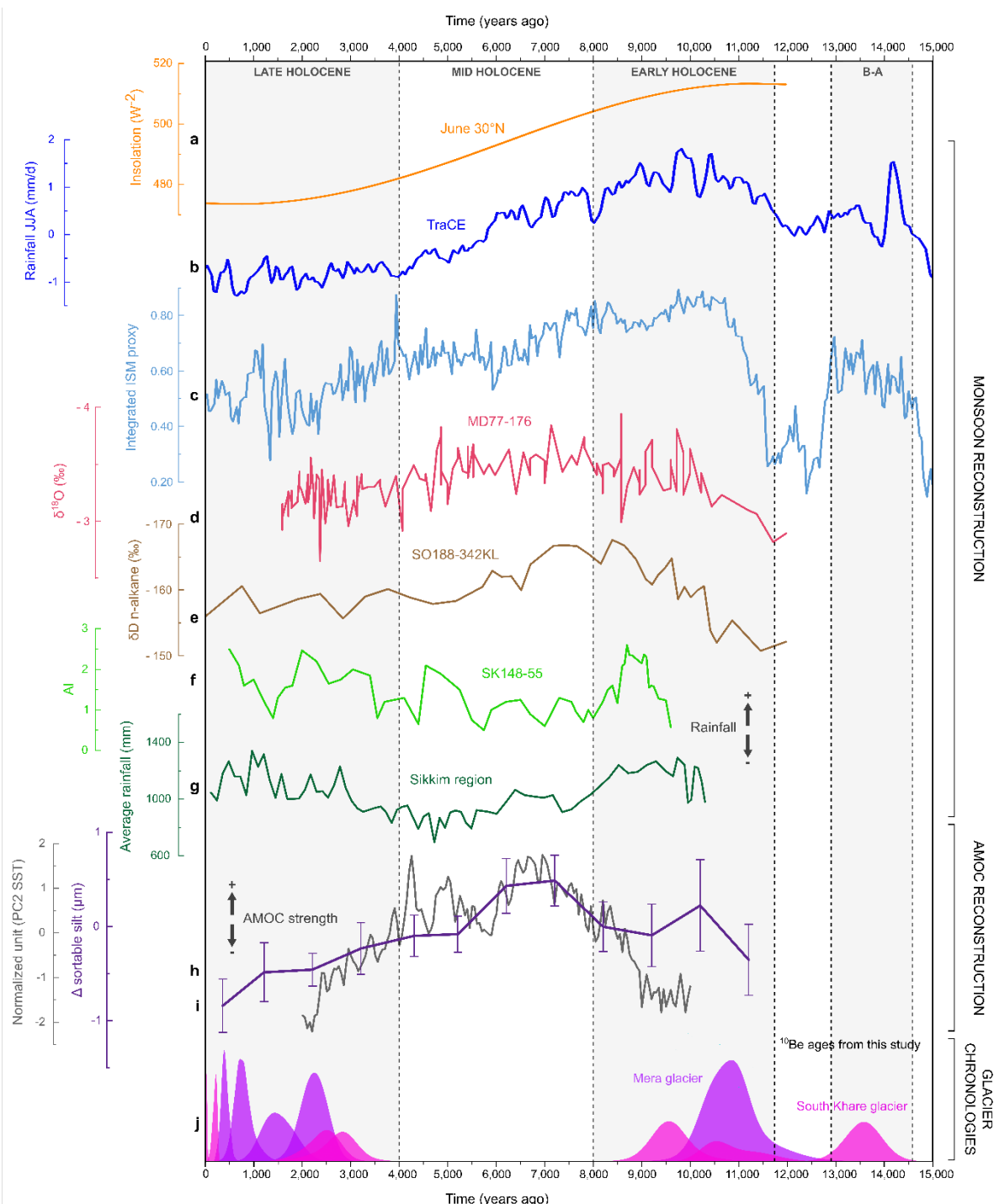


Figure 6. Some glacial chronologies in Himalaya and summer precipitation. a). The chronologies are plotted on the regional atmospheric High Asia Refined analysis (after Wang et al., 2020) showing precipitation amount in June, July and August; b). Circle shows a CRE moraine age with total uncertainty from a debris-free glacier. Rectangle shows a moraine with total uncertainty from a debris-covered glacier. N°1, Kashmir after Shaha et al. (2019); n°2-3 Garwhal after Barnard et al. (2004) and Murari et al. (2014) respectively; n°4 Ganesh region (central Nepal) after Gayer et al. (2006); n°5 Langtang Himal after Barnard et al. (2006); n°6-

540 8 Khumbu valley (Nepal) after Finkel et al. (2003) and Hornsey et al. (2022), n°9-10 Mera and
 541 South Kare glaciers this study (see text for further information).



542
 543 **Figure 7.** Nepalese glacier chronologies compared to climate proxies. a). Summer insolation
 544 changes at 30°N; b). precipitation changes (referenced the mean over the whole Holocene)
 545 during the wet season (JJA) from TraCE full forcing experiment (Liu et al., 2009). c). Monsoon

reconstruction from a compilation of stalagmite $\delta^{18}O$ from 14 caves (Yu et al., 2022). d). Monsoon reconstruction from marine core MD 177-176 in the Gulf of Bengal after Marzin et al (2013). e). Monsoon reconstruction from SO188-342KL in the Gulf of Bengal after Contreras-Rosales et al. (2014). f). Monsoon reconstruction from sediment core SK 148-55 in Arabian Sea after Thamban et al. (2007). g). Annual precipitation reconstruction from a sediment core in Sikkim region after Ali et al. (2018). h). and i). AMOC reconstructions from Thornalley et al. (2013) and Ayache et al. (2018). j). ^{10}Be CRE age probability density distributions with their analytical uncertainties during the Holocene from mountain glaciers of the investigated Mera (purple shaded curves) and South Khare glaciers. Grey vertical rectangles show major chronozones.

5-3 Comparison with other glacier chronologies in the HMA

Comparing Mera and South Khare glacier chronologies with other glaciers in the HMA does not provide robust conclusions (Finkel et al., 2003; Owen et al., 2009; Saha et al., 2019). Indeed, glacial chronologies covering the investigated Lateglacial-Holocene period without undated moraine that may have been formed during this time remain very rare ($n < 10$). Moreover, these rare cases do not exhibit a clear regional pattern whatever the type of glaciers considered (debris-free or debris-covered) with a specific glacier evolution in dominated westerlies or monsoonal regions. For instance, in Garhwal Himalaya, glaciers from Bhagirathi valley ($n^{\circ}2$ Fig. 6, Barnard et al., 2004) may have an in-phase evolution (maximum extent in the Early Holocene) with debris-free glaciers reported in this study. However, glaciers in Kashmir, or in Langtang Himal (Barnard et al., 2006; Murari et al., 2014; Saha et al., 2018) (Figs.1,6), would have another long-term Holocene evolution with a maximum extent asynchronous with that reported in this study. As mentioned earlier, current observations suggest a strong mass balance variability driven by the respective influence of precipitation and

temperature on glacier mass balance (Sakai and Fujita, 2017; Brun et al., 2017). Here we hypothesize that the strong heterogeneity of glacier fluctuations in the past reflects the current heterogeneity of glacier sensitivity to climate conditions as well as the spatial variability of climate change at the scale of the Asian continent.

5-4 An unresolved relationship between climate forcings and the observed trend of the two debris-free glaciers during the Holocene

Multi centennial glacier fluctuations documented by ^{10}Be moraine records reported in this study revealed a possible large glacial extent during the Bølling/Allerød (at the base of SK glacier) and two other large glacier advances, recorded on both glaciers, during the Early and Late Holocene, respectively. The formation of SK-M5 during the B/A corresponds to an enhanced period of precipitations reported by TraCE model and a recent compilation of stalagmite $\delta^{18}\text{O}$ data from a total of 14 caves (Yu et al., 2022) spanning 0° – 35°N , 70° – 95°E , that establish a continuous integrated ISM proxy record. However on both records this does not correspond to the maximum of precipitation that occurred during the Early Holocene instead (Fig. 7). Consequently, it remains unclear why SK-M5 is the largest advance while it did not occur during the maximum of precipitation and why we did not observe such an advance on Mera glaciers. Thus we will not further explore possible climate conditions that would explain the formation of this moraine. However, we will discuss the possible climate forcings during the Holocene that may cause the observed large extension during the Early Holocene and the second large advance period occurring in the Late Holocene. For the present-day, the two debris-free glaciers investigated in this study are driven during the wet season on the one hand by precipitation from the Bay of Bengal and on the other hand by temperatures that impact the altitude of the snow/rain phase (Litt et al., 2019; Wagon et al., 2021). We will thus focus

successively on these two potential driving factors throughout the Holocene using climate model results and proxy data.

It is generally considered that a strong ISM occurs during summer insolation maxima and causes enhanced precipitation to the Himalaya (Rachid et al., 2011). By contrast, reduced precipitation related to a weak monsoon occurs during cold periods and weak summer insolation. In a simple way these two large advance periods during the Early and Late Holocene should be explained by an increase in precipitation compared with that during the Mid-Holocene during which these two glaciers are supposed to have retreated.

The evolution of precipitation simulated by the full forcing experiments revealed after a maximum in the Early Holocene a progressive decrease throughout the rest of the Holocene (Fig. 7b). None of TraCE and LOVECLIM model simulations show precipitation variations that perfectly fit with the two glacier moraine records investigated in this study. While a maximum ISM in the Early Holocene is concomitant with our moraine records, the simulated evolution of climate conditions during the Mid and Late Holocene cannot simply explain glacier evolution. Causes for this discrepancy can be multiple and might notably be linked to biases in the models. Indeed, from a multi-configuration ensemble of up-to-date fully coupled global transient simulations covering the last 6 ka, Cretat et al (2020) evidenced several model-dependent issues. Tests conducted over the 20th century show that the vegetation–climate interactions modulate the timing of the monsoon onset in the model which can be shifted by more than two months compared to observations. The location of the 2 mm/day isohyet from April to September shows remarkable differences between observations and their simulations. Moreover, differences between observations and their simulations in the variability of monsoon rainfall can exceed 30%. Over the last 6 ka, the drying trend from the Mid-Holocene including extremes, and a contraction of the rainy season evidenced in the IPSL model is larger in

simulations with higher horizontal resolution of the atmosphere and improved land surface hydrology. In addition, Mid to Late Holocene changes in JJAS rainfall mean-state documented in the IPSL model show an extraordinary spatial variability with regions where the drying trend is more significant than others.

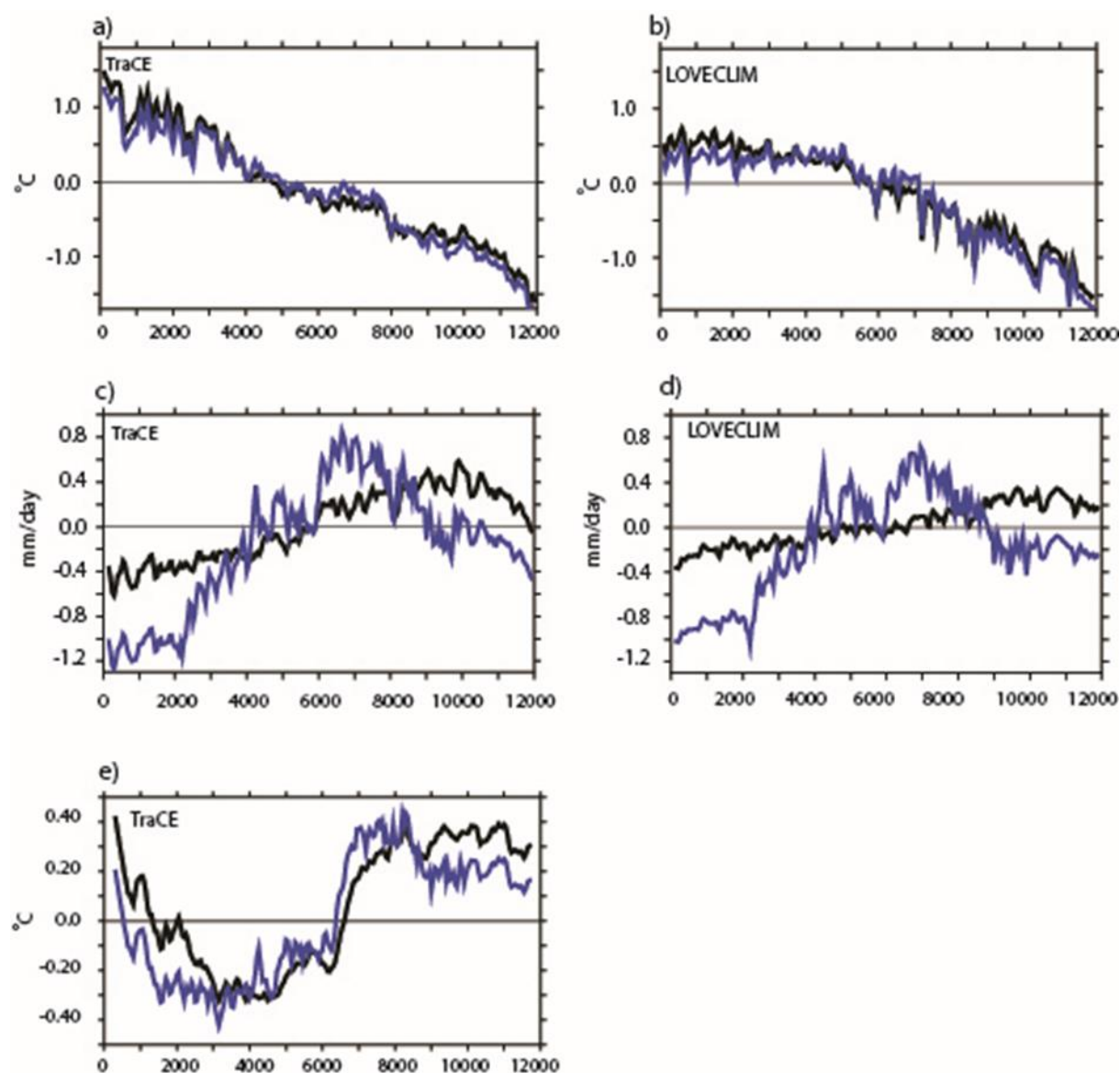


Figure 8. Estimates of temperature and precipitation in Mera region from the two GCMs TraCE and LOVECLIM (full forcing experiments). Black line shows the raw data from the two

models, the blue line shows AMOC corrected data at an annual time scale, a,b,c,d and e) at a seasonal time scale (JJA). All time series have referenced the mean over the period 2-10 ka BP.

As precipitation is a key driver of the investigated glaciers, we explore the reconstructions of paleo-precipitation of the ISM to see if they agree with climate model simulations and can explain the glacier evolution. Unfortunately, terrestrial and marine paleo-precipitation records are rare and do not perfectly correlate with model results and moraine records (Rachid et al., 2011). For instance, MD77-176 core located in the Bay of Bengal (14°31'0 N, 93°08'0 E, Fig.1) (Marzin et al., 2013) indicates enhanced monsoon rains over the Indian subcontinent between 11-8 ka followed by a progressive decrease during the rest of the Holocene (Fig. 7d), in contrast with the general pattern from TraCE simulation (Fig. 7b). A similar pattern of change is shown from a sediment core SO188-342KL (19° 97' N, 90° 03' E; Contreras-Rosales et al., 2014) in the Bay of Bengal.

Hypothesizing that the current major source of precipitation falling on Mera glacier from the Bay of Bengal may not be stationary through time (Ali et al., 2018), we thus explored other oceanic and terrestrial monsoon precipitation reconstructions from the Arabian Sea and India respectively (Grupta et al., 2005; Ali et al., 2019; Banerji et al., 2020). However again, none of their results agree with our paleo moraine records (see for instance the sediment core SK148-55 from Thamban et al., 2007 Fig. 7f). Thus, the maximum ISM in the Early Holocene documented both in the composite record of stalagmite $\delta^{18}\text{O}$ data from a total of 14 caves (Fig. 7c) (Yu et al., 2022) and in the models agrees with the maximum glacier extent, while there would be a divergence for the rest of the Holocene. In addition, a remarkable exception comes from reconstructed precipitation from a glacial outwash sedimentary profile in Chopta valley, Sikkim Himalaya (located east of the Khumbu region). Here Ali et al. (2018) showed humid periods that roughly match with our moraine records (Fig. 7g). Indeed, the authors identified

two periods of unstable climate conditions with higher precipitation during the Early (between 10.6-8 ka) and Late Holocene (between 2.9-0.3 ka) respectively, interrupted by dry conditions during the Mid-Holocene. Furthermore, the authors inferred, in agreement with some recent studies (e.g. Sun et al., 2012; Marzin et al., 2013), that the ISM precipitation reconstruction was linked to variations in the North Atlantic climate on multi centennial to millennial time scales, with the AMOC being a potential driver of these changes in North Atlantic climate and its teleconnection with the ISM (e.g. Marzin et al., 2013).

As AMOC forcing is known to interact with monsoon (IPCC SROCC 2019), we thus investigated the possible influence of this AMOC forcing on our moraine records. Interestingly, recent reconstruction of AMOC changes revealed two weak AMOC periods during the Early and Late Holocene respectively (Thormaley et al., 2013; Ayache et al., 2018). To further explore this possible influence of AMOC on the ISM and more generally, on the two debris-free glaciers' evolution during the investigated period, we first extracted regional precipitation series at an annual time scale and during the wet season (JJA) from the two full forcing transitory simulations that cover the Holocene simulated by CCSM4 TraCE and LOVECLIM climate models. As AMOC is poorly represented in these two models during the Holocene (Jomelli et al., 2022), we used AMOC reconstructions to compute corrected GCMs precipitation changes over the Holocene according to the method described in Jomelli et al. (2022) (Fig. 8). AMOC corrected monsoon precipitation changes show strong variations with a progressive increase in precipitation culminating during the Mid-Holocene followed by a progressive decrease. Interestingly, these AMOC-corrected precipitation changes (Fig. 8 blue curves) show a good correspondence with precipitation from proxy records in the Bay of Bengal (Fig. 7d, e). This precipitation pattern of the AMOC-corrected precipitation is in line with various modeling results, showing a stronger ISM when the AMOC and the North Atlantic is warmer (e.g. Jackson et al. 2015). However, this pattern does not show a good correspondence

with our moraine records since it is going in the opposite directions to what might be required to explain precipitation-driven increase in the glaciers, (i.e. an increase in precipitation).

Temperature variations would be superimposed on the precipitation evolution. We may also consider that the impact of the two variables (precipitation and temperature) on the glacier would be opposite stronger monsoon (positive influence on mass balance) associated with warmer temperature (negative influence on mass balance) while the influence of temperature could be compensated by an increase in precipitation. However, here again none of TraCE and LOVECLIM model simulations show temperature variations that perfectly fit with the two glacier moraine records investigated in this study (Figs 7, 8).

All in all, the relationships between climate conditions and long-term glacier changes in the investigated sector of Nepal remain puzzling, and reveal potential issues in the modeling of climate conditions, which could be related to the regional climatic responses in this mountainous region. For instance, due to extreme topography, a large spatial variability of precipitation is currently observed in the central Himalaya, leading to very different precipitation trends over short distances; this is still not captured by models. Moreover, the mass balance sensitivity is highly dependent on the total annual precipitation and therefore may have changed over the Holocene. Finally, the major source of precipitation falling on Mera glacier has potentially changed over time, making it impossible to find a clear relationship between regional climate change and local glacier evolution. To overcome such issues, teleconnections between AMOC and climate conditions in Mera region need further investigations as dynamic downscaling in particular, but this remains beyond the scope of this study. In addition, new moraines chronologies from debris-free glaciers across the mountain

range may help to identify a regional trend confirming or negating the evolution of Mera and South Kare glaciers.

6- Conclusion

We documented the evolution of the two debris-free Mera and South Khare glaciers during the end of the Lateglacial and the Holocene in the central Himalaya from 51 cosmogenic ^{10}Be surface exposure ages of samples collected from boulders on moraines and from roche moutonnées. Mera glacier is of particular interest because an energy and mass balance monitoring has been conducted since 2007 enabling a deeper understanding of glacier climate relationships over the recent period. These instrumental measurements indicate that the glaciers' mass balances are driven during the wet summer season (*i*) by precipitation from the Bay of Bengal and (*ii*) by temperatures that impact the altitude of the snow/rain phase.

Our paleo glaciological investigations revealed that South Khare glacier evidenced a large glacier extent during the Bølling/Allerød. But glacier advance during this period remains puzzling and new records are needed to better understand climate drivers. On both glaciers ^{10}Be CRE ages also revealed the existence of Early Holocene moraines and attest of their maximum size at that time over the last 11.6 ka. Moreover, the lack of moraine dated to the Mid-Holocene and ^{10}Be inheritance for some roche moutonnées at the base of the current ice front positions suggest the two glaciers were smaller during the Mid-Holocene than during the Late Holocene. From about 3 ka several advances were recorded, which were larger than the LIA.

Current observations suggest both glaciers were driven on the one hand by ISM precipitation, and on the other hand by temperature. During the Holocene, these two variables might have been sensitive to summer insolation changes and AMOC changes among other factors. Strong spatial precipitation variability is also evidenced suggesting possible differences between moraine records and proxies or regional precipitation changes estimated from climate

models. However, we did not see any ISM precipitation and temperature changes documented from most proxy records and climate model simulations that would perfectly explain the reconstructed glacier changes presented in this study. If the maximum glacial extent is concomitant with enhanced ISM documented from models and some proxy records, the Late Holocene glacier advance remains puzzling. We, therefore, claim that new glacio-geomorphological data combined with improved GCMs output are necessary to get a better understanding of glacier climate relationships in the past in this region.

Acknowledgments

The ASTER AMS national facility (CEREGE, Aix-en-Provence) is supported by the INSU/CNRS, the ANR through the “Projets thématiques d’excellence” program for the “Equipements d’excellence” ASTER-CEREGE action and IRD. Field work, and mass and energy balance results have been supported by the French Service d’Observation GLACIOCLIM, part of IR OZCAR. This work would not have been possible without the support of the IRD International Joint Lab WATER-HIMAL (PIs: D. Shrestha, and P. Wagnon) and all the efforts from people in the field: porters, students, helpers, colleagues who are greatly acknowledged here. T. de Garidel and F. Bassino are also warmly acknowledged for their help with ISM data reconstructions.

References

- Ali, S.N., Dubey, J., Ghosh, R., Quamar, M. F., Sharma, A., Morthekai, P., Dimri, A. P., Shekhar, M., Arif, M., Agrawal. S., 2018. High frequency abrupt shifts in the Indian summer monsoon since Younger Dryas in the Himalaya. *Scientific Reports*, 8(1), 1–8.
- Ali, S.N., Dubey, J., Shekhar, M., Morthekai, P., 2019. Holocene Indian Summer Monsoon variability from the core monsoon zone of India, a pollen-based review. *Grana* 58, 311-327.

753 Arnold, M., Merchel, S., Bourlès, D. L., Braucher, R., Benedetti, L., Finkel, R.C., Aumaître,
 754 G., Gottdang, A., Klein, M., 2010. The French accelerator mass spectrometry facility ASTER:
 755 improved performance and developments Nuclear Instrumentation Methods in Physics
 756 Research Section B: Beam Interactions with Materials and Atoms 268, 1954–1959.

757 Ayache, M., Swingedouw D., Mary Y., Eynaud F., Colin C., 2018. Multi-centennial variability
 758 of the AMOC over the Holocene: A new reconstruction based on multiple proxy-derived SST
 759 records. Global and Planetary Change 170, 173-183.

760 Azam, M.F., Kargel, J.S., Shea, J.M., Nepal, S., Haritashya, U.K., Srivastava, S., Maussion, F.,
 761 Qazi, N., Chevallier, P., Dimri, A.P., Kulkarni, A.V., Cogley, J.G., Bahuguna, I., 2021.
 762 Glaciohydrology of the Himalaya-Karakoram. Science 373 (6557) doi:
 763 10.1126/science.abf3668.

764 Balco, G., Stone, J.O., Lifton, N.A., Dunai, T.J., 2008. A complete and easily accessible means
 765 of calculating surface exposure ages or erosion rates from ^{10}Be and ^{26}Al measurements. Quat.
 766 Geochronol. 3 (3), 174–195.

767 Banerji, U. S., Arulbalaji, P., Padmalal. D., 2020. Holocene climate variability and indian
 768 summer monsoon: an overview. The Holocene 30, 766-773.

769 Barnard, P.L. Owen, L.A. Finkel, R.C., 2004. Style and timing of glacial and paraglacial
 770 sedimentation in a monsoon-influenced high Himalayan environment, the upper Bhagirathi
 771 Valley, Garhwal Himalaya [Sedimentary Geology](#) 165,199-221.

772 Barnard, P.L. Owen, L.A. Finkel, R.C., Asahi. K., 2006. Landscape response to deglaciation in
 773 a high relief, monsoon-influenced alpine environment, Langtang Himal, Nepal. Quaternary
 774 Science Reviews, 25, 2162-2176.

775 Batbaatar, J., Gillespie, A.R., Fink, D., Matmon, A., Fujioka, T., 2018. Asynchronous
 776 glaciations in arid continental climate. Quaternary Science Reviews, 182, 1-19.

777 Bonekamp, P.N.J., de Kok, R.J., Collier, E., Immerzeel, W.W., 2019. Contrasting
778 Meteorological Drivers of the Glacier Mass Balance Between the Karakoram and Central
779 Himalaya. *Front. Earth Sci.* 7:107. doi: 10.3389/feart.2019.00107

780 Bookhagen, B., Burbank, D.W., 2006. Topography, relief and TRMM-derived rainfall
781 variations along the Himalaya. *Geophys. Res. Lett.*, 33, L08405, doi:10.1029/2006GL026037

782 Borchers, B., Marrero, S., Balco, G., Caffee, M., Goehring, B., Lifton, N., Nishiizumi, K.,
783 Phillips, F., Schaefer, J., John Stone, J., 2016. Geological calibration of spallation production
784 rates in the CRONUS-Earth project. *Quat Geochro.* 31, 188-198.

785 Braucher, R., Guillou, V., Bourlès, D. L., Arnold, M., Aumaître, G., Keddadouche, K., Nottoli
786 E., 2015. Preparation of Aster in-house 10be/9be standard solutions. *Nuclear Instruments and*
787 *Methods in Physics Research B*, 361:335–340.

788 Brun, F., Berthier, E., Wagnon, P., Kääb, A., Treichler, D., 2017. A spatially resolved estimate
789 of high mountain Asia glacier mass balances from 2000 to 2016. *Nature Geoscience*, 10:668–
790 673.

791 Brun, F., Wagnon, P., Berthier, E., Jomelli, V., Maharjan, S.B., Shrestha, F. Kraaijenbrink P.
792 D.A., 2019. Heterogeneous influence of glacier morphology on the mass balance variability in
793 high mountain Asia. *Journal of Geophysical Research: Earth Surface*, 121(6):1331–1345.

794 Cheng, H., Zhang, H., Christoph Spötl, C., Baker, J., Sinha, A., Li, H., Bartolomé, M., Moreno,
795 A., Kathayat, G., Zhao, J., Dong, X., Li, Y., Ning, Y., Jia, X., Zong, B., Ait Brahim, Y., Pérez
796 Mejías, C., Cai, Y., Novello, V.F., Cruz, F.W., Severinghaus, J.P., An, Z., Edwards, R.L., 2020.
797 Timing and structure of the Younger Dryas event and its underlying climate dynamics. *PNAS*
798 117, 38. <https://doi.org/10.1073/pnas.200786911>.

799 Chmeleff, J., von Blanckenburg, F., Kossert, K., Jakob, D., 2010. Determination of the 10Be
800 half-life by multicollector ICP-MS and liquid scintillation counting. *Nucl. Instrum. Methods*
801 *Phys. Res., Sect. B* 268 (2), 192–199.

802 Clark, P.U., Dyke, A.S., Shakun, J.D., Carlson, A.E., Clark, J., Wohlfarth, B., Mitrovica, J.X.,
 803 Hosteler, S.W., Mc Cabe, A.M., 2009. The last glacial maximum. *Science* 325, 710-714.
 804 Contreras-Rosales L.A., Jennerjahn, T., Tharammal, T., Meyer, V., Lückge, A., Paul, A.,
 805 Schefus E., 2014. Evolution of the Indian Summer Monsoon and terrestrial vegetation in the
 806 Bengal region during the past 18 ka. *Quaternary Sci. Rev.* 102, 133-148.
 807 Crétat, J., Braconnot, P., Terray, P., Marti, O., Falasca, F., 2020. Mid-Holocene to present-day
 808 evolution of the Indian monsoon in transient global simulations. *Climate Dynamics*, 55, 2761–
 809 2784.
 810 Dunai, T., 2010. *Cosmogenic Nuclides. Principles, concepts and application in the Earth*
 811 *surface Sciences*. Cambridge, 188pp.
 812 Finkel, R.C., Owen, L.A., Barnard, P.L., Caffee, M.W., 2003. Beryllium-10 dating of Mount
 813 Everest moraines indicates a strong monsoonal influence and glacial synchronicity throughout
 814 the Himalaya. *Geology* 31, 561–564.
 815 Fugger, S., C. L., Fyffe, C.L., Fatichi, S., Miles, E., McCarthy, M., Shaw, T.E., Ding, B., Yang,
 816 W., Wagnon, P., Immerzeel, W., Liu, Q., Pellicciotti, F., 2021. Understanding monsoon control
 817 on the mass and energy balance of Himalayan glaciers. *The Cryosphere* 16, 1641-1652.
 818 Gayer, E., Lavé, J., Pik, R., France-Lanord, C., 2006. Monsoonal forcing of Holocene glacier
 819 fluctuations in Ganesh Himal (Central Nepal) constrained by cosmogenic ³He exposure ages of
 820 garnets. 2006. *Earth and Planetary Science Letters* 252, 275–288.
 821 Gibbons, A. B., Megeath, J. D., Pierce, K. L., 1984. Probability of moraine survival in a
 822 succession of glacial advances. *Geology* 12, 327–330.
 823 Gupta, A.K., Das, M., Anderson, D.M., 2005. Solar influence on the Indian summer monsoon
 824 during the Holocene. *Geophysical Research Letters*, 32, L17703, doi:10.1029/2005GL022685.
 825 Hornsey, J., Rowan, A. V., Kirkbride, M., Livingstone, S.T., Fabel, D., Rodes, A., Quincey,
 826 D.J., Hubbard, B., Jomelli, V., 2022. Be-10 dating of ice-marginal moraines in the Khumbu

827 Valley, Nepal, Central Himalaya, reveals the response of monsoon-influenced debris-covered
828 glaciers to Holocene climate change. JGR under review.

829 Hugonnet, R., McNabb, R., Berthier, E., Menounos, B., Nuth, C., Girod, L., Farinotti, D., Huss,
830 M., Dussaillant, I., Brun, F., and Kääb, A., 2021. Accelerated global glacier mass loss in the
831 early twenty-first century. *Nature*, 592, 726-731.

832 Jackson, L. C. Kahana, R., Graham, T., Ringer, M.A., Woollings, T., Mecking, J.V., Wood, R.
833 A., 2015. Global and European climate impacts of a slowdown of the AMOC in a high resolution
834 GCM. *Clim. Dyn.* 45, 3299–3316.

835 Jomelli, V., Francou, B., 2000. Comparing characteristics of rockfall talus and snow avalanche
836 landforms in an alpine environment using a new methodological approach. *Geomorphology*,
837 35, 181-192.

838 Jomelli, V., Swingedouw D., Vuille, M., Favier, V., Goehring, B., Shakun, J., Braucher, R.,
839 Schimmelpfennig I., Menviel, L., Rabatel, A., Martin, L.C.P., Blard, P-H., Condom, T., Lupker,
840 M., Christl, M., He, Verfaillie, D., Z., Gorin, A., ASTER Team. 2022. AMOC control on
841 millennial-scale glacier changes during the Holocene. *Nature com*, doi.org/10.1038/s41467-
842 022-28939-9

843 Kaufman, D., and 102 others 2020. A global database of Holocene paleo temperature records.
844 *Scientific Data* 7, 115, <https://doi.org/10.1038/s41597-020-0445-3>.

845 Khadka A, Wagnon, P., Shrestha, D., Brun, F., Koch, I., 2022 Validation of ERA5 Land Data
846 in the Upper Dudh-Koshi Region and its implication for Energy/Mass balance, *J. Applied*
847 *Meteo.*, 61(8)DOI: 10.1175/JAMC-D-21-0091.1

848 Kobashi, T., Menviel, L., Jeltsch-Thömmes, A., Vinther, B. M., Box, J. E., Muscheler, R.,
849 Nakaegawa, T., Pfister, P. L., Döring, M., Leuenberger, M., Wanner, H., Ohmura, A., 2017:
850 Volcanic influence on centennial to millennial Holocene Greenland temperature change.
851 *Scientific Reports* 8, 1, 4292.

852 Korschinek, G., Bergmaier, A., Faestermann, T., Gerstmann, U.C., Knie, K., Rugel, G.,
 853 Wallner, A., Dillmann, I., Dollinger, G., von Gostomski, Ch.L., Kossert, K., Maiti, M.,
 854 Poutivtsev, M., Remmert, A., 2010. A new value for the half-life of ^{10}Be by Heavy-Ion Elastic
 855 Recoil Detection and liquid scintillation counting. Nuclear Instruments and Methods in Physics
 856 Research Section B: Beam Interactions with Materials and Atoms 268, 2, 187–191:
 857 doi:10.1016/j.nimb.2009.09.020.
 858 Lal, D., 1991. Cosmic ray labeling of erosion surfaces: *in situ* nuclide production rates and
 859 erosion models. Earth and Planetary Science Letters 104, 2–4, 424–439: doi:10.1016/0012-
 860 821X(91)90220-C.
 861 Lifton, N., Sato, T., Dunai, T.J., 2014. Scaling in situ cosmogenic nuclide production rates using
 862 analytical approximations to atmospheric cosmic-ray fluxes. Earth Planet. Sci. Lett. 386, 149–
 863 160. <https://doi.org/10.1016/j.epsl.2013.10.052>.
 864 Litt, M., Shea, J., Wagnon, P., Steiner, J. Koch, I. Stigter, E., Immerzeel. W., 2019. Glacier
 865 ablation and temperature indexed melt models in the nepalese himalaya. Scientific Reports,
 866 9(1).1–10.
 867 Liu, Z., Otto-Bliesner, B.L., Hee, F., Brady, E.C. Tomas, R., Clark, P.U., Carlson, A.E., Lynch-
 868 Steiglitz, J., Curry, W., Brook, E., Erickson, D., Jacob, R., Kutzbach, J., Cheng, J., 2009.
 869 Transient simulation of deglacial Climate Evolution with a new mechanism for Bolling-Allerod
 870 warming. Science 325, 310-314.
 871 Martin, L. C. P., Blard, P.-H., Balco, G., Lave, J., Delunel, R., Lifton, N., Laurent, V., 2017.
 872 The CREp program and the ICE-D production rate calibration database: a fully parameterizable
 873 and updated online tool to compute cosmic-ray exposure ages. Quaternary Geochronology 38,
 874 25–49.

875 Marzin, C., Kallel, N. Kageyama, M., Duplessy, J. C., Braconnot, P., 2013. Glacial of the Indian
876 monsoon and their relationship with North Atlantic climate: New data and fluctuations and
877 modelling experiments. *Climate of the Past* 9, 2135–2151.

878 Matthews, T., Perry, L. B., Koch, I., Aryal, D., Khadka, A., Shrestha, D., Abernathy, K., Elmore,
879 A. C., Seimon, A., Tait, A., Elvin, S., Tuladhar, S., Baidya, S. K., Potocki, M., Birkel, S.
880 D., Kang, S., Sherpa, T. C., Gajurel, A., Mayewski, P. A., 2020. Going to Extremes: Installing
881 the World's Highest Weather Stations on Mount Everest, *B. Am. Meteorol. Soc.*, 101, E1870–
882 E1890, <https://doi.org/10.1175/BAMS-D-19-0198.1>, 2020.

883 McKay, N.P., Kaufman D.S., Routson C.C., Erb M.P., Zander P.D., 2018. The Onset and Rate
884 of Holocene Neoglacial Cooling in the Arctic. *GRL* 45, doi.org/10.1029/2018GL079773

885 Merchel, S., Bremser, W., Alfimov, V., Arnold, M., Aumaître, G., Benedetti, L., Bourles, D.L.,
886 Caffee, M., Fifield, L.K., Finkel, R.C., Freeman, S.P.H.T., Martschini, M., Matsushi, Y., Rood,
887 D.H., Sasa, K., Steier, P., Takahashi, T., Tamari, M., Tims, S.G., Tosaki, Y., Wilcken, K.M.,
888 Xu, S., 2011. Ultra-trace analysis of ^{36}Cl by accelerator mass spectrometry: an interlaboratory
889 study. *Anal. Bioanal. Chem. Res.* 400, 3125–3132.

890 Mölg, T., Maussion, F., Scherer, D., 2014. Mid-latitude westerlies as a driver of glacier
891 variability in monsoonal High Asia. *Nat. Clim. Change* 4, 68–73.

892 Murari, M.K., Owen, L.A., Dortch, J.M., Caffee, M.W., Dietsch, C., Fuchs, M., Haneberg,
893 W.C., Sharma, M.C., Townsend-Small, A., 2014. Timing and climatic drivers for glaciation
894 across monsoon-influenced regions of the Himalayan–Tibetan orogen. *Quaternary Sci. Rev.*
895 88, 159–182.

896 Owen, L.A., 2009. Latest Pleistocene and Holocene glacier fluctuations in the Himalaya and
897 Tibet. *Quaternary Sci. Rev.* 28, 2150–2164.

898 Owen, L.A., Finkel, R.C., Barnard, P.L., Haizhou, M., Asahi, K., Caffee, M.W., Derbyshire,
899 E., 2005. Climatic and topographic controls on the style and timing of Late Quaternary

900 glaciation throughout Tibet and the Himalaya defined by ^{10}Be cosmogenic radionuclide
 901 surface exposure dating. *Quaternary Sci. Rev.* 24, 1391–1411.

902 Owen, L.A., Caffee, M.W., Finkel, R.C., Seong, B.Y., 2008. Quaternary glaciations of the
 903 Himalayan–Tibetan orogen. *Journal of Quaternary Science* 23, 513–532.

904 Owen, L.A., Robinson, R., Benn, D.I., Finkel, R.C., Davis, N.K., Yi, C., Putkonen, J., Li, D.,
 905 Murray, A.S., 2009. Quaternary glaciation of Mount Everest. *Quaternary Sci. Rev.* 28, 1412–
 906 1433.

907 Owen, L.A., Dortch, J.M., 2014. Nature and timing of Quaternary glaciation in the Himalayan–
 908 Tibetan orogen. *Quaternary Sci. Rev.* 88, 14–54.

909 Perry, L. B., Matthews, T., Guy, H., Koch, I., Khadka, A., Elmore, A.C., Shrestha, D.,
 910 Tuladhar, S., Baidya, S.K., Maharjan S., Wagnon, P., Aryal, D., Seimon, A., Gajurel, A.,
 911 Mayewski, P. A., 2020. Precipitation characteristics and moisture source regions on Mt. Everest
 912 in the Khumbu, Nepal. *One Earth* 3, 594–607.

913 Pritchard, H. D., 2019. Asia’s shrinking glaciers protect large populations from drought stress.
 914 *Nature* 569, 649–654.

915 Rashid, H., England, E., Thompson, L Polyak L., 2011. Late glacial to holocene indian summer
 916 monsoon variability based upon sediment records taken from the bay of bengal. *Terrestrial,*
 917 *Atmospheric and Oceanic Sciences*, 22, 215–228.

918 Rowan, A. V., 2016. The ‘Little Ice Age’ in the Himalaya: a review of glacier advance driven
 919 by Northern Hemisphere temperature change. *The Holocene* 27, 292–308.

920 Rowan, A.V., Egholm, D.L., Quincey, D.J., Glasser, N.F., 2015. Modelling the feedbacks
 921 between mass balance, ice flow and debris transport to predict the response to climate change
 922 of debris covered glaciers in the Himalaya. *Earth and Planetary Science Letters* 430, 427–438.
 923 <https://doi.org/10.1016/j.epsl.2015.09.004>

924 Saha, S., Owen, L.A. Orr, E.N., Caffee. M.W., 2018. Timing and nature of holocene glacier
 925 advances at the northwestern end of the himalayan-tibetan orogen. *Quaternary Sci. Rev.*
 926 187,177–202,

927 Saha, S., Owen, L.A. Orr, E.N., Caffee. M.W., 2019. Cosmogenic ¹⁰be and equilibrium-line
 928 altitude dataset of holocene glacier advances in the himalayan-tibetan orogen. *Data in Brief*,
 929 26:104412. <https://doi.org/10.1016/j.dib.2019.104412>

930 Saha, S., Owen, L.A., Orr, E.N., Caffee M.W., 2019. High-frequency Holocene glacier
 931 fluctuations in the Himalayan Tibetan orogen. *Quaternary Sci. Rev.* 220, 372-400.

932 Sakai, A., Fujita, K., 2017. Contrasting glacier responses to recent climate change in high
 933 mountain Asia. *Scientific Reports* 7, 13717 | DOI:10.1038/s41598-017-14256-5

934 Sherpa, S. F., Wagnon, P., Brun, F., Berthier, E., Vincent, C., Lejeune, Y., Arnaud, Y.,
 935 Kayastha, R., Sinisalo, A., 2017. Contrasted surface mass balances of debris-free glaciers
 936 observed between the southern and the inner parts of the Everest region (2007-2015). *J. Glaciol*,
 937 doi: 10.1017/jog.2017.30

938 Seong, Y.B., Owen, L.A., Bishop, M.P., Bush, A., Clendon, P., Copland, L., Finkelf, R., Kamp,
 939 U., Shroder Jr., J.F., 2007. Quaternary glacial history of the Central Karakoram. *Quaternary*
 940 *Sci. Rev* 26, 3384–3405.

941 Stigter, E.E., Litt, M., Steiner, J.F., Bonekamp, P.N.J., Shea, J.M., Bierkens, M.F.P.,
 942 Immerzeel, W.W., 2018. The Importance of Snow Sublimation on a Himalayan Glacier. *Front.*
 943 *Earth Sci.* 6:108. doi: 10.3389/feart.2018.00108

944 Stigter, E.E., Steiner, J.F., Koch, I., Saloranta, T.M., Kirkham, J.D., Immerzeel, W.W., 2021.
 945 Energy and mass balance dynamics of the seasonal snowpack at two high-altitude sites in the
 946 Himalaya. *Cold Regions Science and Technology*, 183, 103233, ISSN 0165-232X,
 947 <https://doi.org/10.1016/j.coldregions.2021.103233>.

948 Solomina, O.N., Bradley, R.S., Hodgson, D.A., Ivy-Ochs, S., Jomelli, V., Mackintosh, A.N.,
 949 Nesje, A., Owen, L.A., Wanner, H., Wiles, G.C., Young, N.E., 2015. Holocene glacier
 950 fluctuations. *Quaternary Sci. Rev.* 111, 9–34.
 951 Solomina, O., Bradley., Jomelli, V., Geirsdottir, A., Kaufman, D., Koch, J., Masiokas, M.,
 952 Miller, G., Nesje, A., Nicolussi, K., Owen, L., Wanner, H., Wiles, G., Yang, B., 2016. Glacier
 953 fluctuations in the last 2000 years. *Quaternary Sci. Rev.* 149, 61-90.
 954 Sun, Y. Clemens, S.C., Morrill, C., Lin, X., Wang, X., An, Z., 2012. Influence of Atlantic
 955 meridional overturning circulation on the East Asian winter monsoon: *Nature Geoscience* 5,
 956 46–49.
 957 Stone, J.O., 2000. Air pressure and cosmogenic isotope production. *Journal of Geophysical*
 958 *Research: Solid Earth* 105, B10, 23753–23759: doi:10.1029/2000JB900181.
 959 Swingedouw, D., Rodehacke, C.B., Behrens, E., Menary, M., Olsen, S.M., Gao, Y.,
 960 Mikolajewicz, U., Mignot, J., Biastoch, A., 2013. Decadal fingerprints of freshwater discharge
 961 around Greenland in a multi-model ensemble. *Clim. Dyn.* 41, 695–720.
 962 Thamban, M., Kawahata, H., Purnachandra Rao, V., 2007. Indian Summer Monsoon
 963 Variability during the Holocene as Recorded in Sediments of the Arabian Sea: Timing and
 964 Implications. *Journal of Oceanography* 63, 1009-1020.
 965 Thornalley, D. J. R., Blaschek, M., Davies, F. J., Praetorius, S., Oppo, D. W., McManus, J. F.,
 966 Hall, I. R., Kleiven, H., Renssen, H., McCave, I.N., 2013. Long-term variations in Iceland–
 967 Scotland overflow strength during the Holocene *Geoscientific Instrumentation Methods and*
 968 *Data Systems* long-term variations in Iceland–Scotland overflow strength during the Holocene.
 969 *Clim. Past* 9, 2073–2084.
 970 Upasana, S.B., Arulbalaji, P., Padmalal, D., 2020. Holocene climate variability and Indian
 971 Summer Monsoon: An overview. *The Holocene* 30,744–773

972 Uppala, S.M., Kållberg, P.W., Simmons, A.J., Andrae, U., Bechtold, V.D.C., Fiorino, M.,
 973 Gibson, J.K., Haseler, J., Hernandez, A., Kelly, G.A., Li, X., Onogi, K., Saarinen, S., Sokka,
 974 N., Allan, R.P., Andersson, E., Arpe, K., Balmaseda, M.A., Beljaars, A.C.M., Berg, L.V.D.,
 975 Bidlot, J., Bormann, N., Caires, S., Chevallier, F., Dethof, A., Dragosavac, M., Fisher, M.,
 976 Fuentes, M., Hagemann, S., Hólm, E., Hoskins, B.J., Isaksen, I., Janssen, P.A.E.M., Jenne, R.,
 977 McNally, A.P., Mahfouf, J.-F., Morcrette, J.-J., Rayner, N.A., Saunders, R.W., Simon, P., Sterl,
 978 A., Trenberth, K.E., Untch, A., Vasiljevic, D., Viterbo, P., Woollen, J., (2005). The ERA-40
 979 re-analysis. *Q.J.R. Meteorol. Soc.*, 131, 2961-3012.
 980 Wagon, P., Vincent, C. Arnaud, Y. Berthier, E. Vuillermoz, E. Gruber, S. Ménégoz, M.
 981 Gilbert, A. Dumont, M., Shea, J. M. Stumm, D., Pokhrel, B. K., 2013. Seasonal and annual mass
 982 balances of Mera and Pokalde glaciers (Nepal Himalaya) since 2007. *Cryosphere*, 7(6):1769–
 983 1786, 2013.
 984 Wagon, P., Brun, F., A. Khadka, A. Berthier, E. Shrestha, D. Vincent, C. Arnaud, Y. Six, D.
 985 Dehecq, A. Ménégoz, M., Jomelli, V., 2021. Reanalysing the 2007–19 glaciological mass-
 986 balance series of mera glacier, Nepal, central Himalaya, using geodetic mass balance. *Journal*
 987 *of Glaciology* 67, 117–125.
 988 Wang, X., Tolksdorf, V., Otto, M., Scherer, D., 2020. WRF-based dynamical downscaling of
 989 ERA5 reanalysis data for High Mountain Asia: Towards a new version of the High Asia Refined
 990 analysis. *International Journal of Climatology*, 41, 742-763. <https://doi.org/10.1002/joc.6686>
 991 Ward G. K., Wilson, S. R., 1978. Procedures for comparing and combining radiocarbon age
 992 determinations: a critique. *Archaeometry* 20, 19–31.
 993 Yan, Q., Owen, L.A., Zhang, Z., Jiang, N., Zhang, R., 2020. Deciphering the evolution and
 994 forcing mechanisms of glaciation over the Himalayan-Tibetan orogen during the past 20,000
 995 years. *EPSL*, 541, DOI: 10.1016/j.epsl.2020.116295

Yu, Z., Colin, C., Wilson, D. J., Bayon, G., Song, Z., Sepulcre, S., Dapoigny, A., Li, Y., Wan, S., 2022. Millennial variability in intermediate ocean circulation and Indian monsoonal weathering inputs during the last deglaciation and Holocene. *Geophysical Research Letters*, 49, e2022GL100003. <https://doi.org/10.1029/2022GL100003>

Tables

Table 1. Cosmogenic data from Mera and South Khare glaciers. The mean age of the landforms is calculated with external uncertainties.

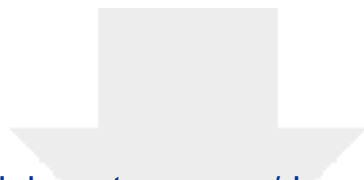
Table 2. Cosmogenic ages calculated using different model schemes. Scaling to the sample locations was made according to the recent, physically-based, LSD model (Lifton et al., 2014) which performs similarly to older empirical models (Borchers et al., 2016). Chosen parameters include the ERA 40 atmospheric reanalysis (Uppala et al., 2005) and the VDM 2016 geomagnetic database.

Competing interests

The authors declare no competing interests

Author contributions

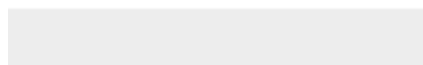
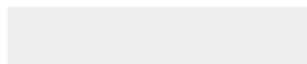
V.J. designed the paper. V.J., PW., F.B., and D.S, realized the field Sampling R.B., J.C., A.H., S.B and V.J. processed the ¹⁰Be sample preparation and analysis. V.J., R.B., J.C., A.H., S.B and ASTER TEAM computed the cosmogenic nuclides ages. D.S. ran the AMOC simulations. V.J., D.S., and P.W. analyzed forcings. V.J. wrote the first draft of the paper and all authors contributed to the discussion and final version of the manuscript.

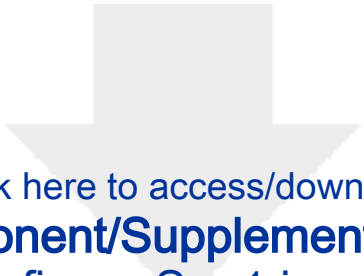


[Click here to access/download](#)


e-Component/Supplementary data

1TABLE_S1 16_12Outlier-Batbaatar way.xlsx





Click here to access/download
e-Component/Supplementary data
figure Sup1.jpg





Click here to access/download
e-Component/Supplementary data
figureSup2.jpg





Click here to access/download
e-Component/Supplementary data
figureSup3.jpg

